

POLYMER MELT VISCOELASTICITY: WHAT WE CAN LEARN FROM MOLECULAR SIMULATIONS

Vlasis G. Mavrantzas

University of Patras, Department of Chemical Engineering

&

FORTH-ICE/HT, Patras GR 26504, Greece

ABSTRACT

In this review, we discuss how computer simulations at molecular level can help understand the complicated mechanics and flow behaviour of polymeric liquids. We focus, in particular, on one of the most distinctive properties of these materials, their viscoelasticity, quantifying the irreversible conversion of the work done for their deformation to heat loss but also their capability to store part of this work as elastic energy. We restrict our analysis to flexible polymers in the melt state and we describe how one can take advantage of recent advances in the field of atomistic Monte Carlo and Molecular Dynamics simulations in order to explain their relaxation mechanisms and flow properties. This information can be used to validate and parameterize molecular models, and to design better constitutive equations capable of providing a reliable expression for the stress tensor in terms of the imposed flow kinematics and certain, well-defined molecular parameters. The availability of such constitutive equations is important in the development of large-scale numerical approaches with predictive power, since they can help reduce the huge number of experiments typically required in industrial applications for optimising materials or for designing new processes and processing technologies.

KEYWORDS: Polymer melt viscoelasticity, GENERIC Monte Carlo, NEMD, atomistic simulation

1. INTRODUCTION

Viscoelasticity refers to the distinctive feature of polymer molecules to exhibit both viscous and elastic properties, the latter associated with the concept of a memory of an "initial" state. The viscous component quantifies the irreversible conversion of part of the work needed for the deformation of polymer molecules to heat whereas the elastic component refers to their ability to store part of this work in the form of elastic energy; this, for example, enables the material to remember its original shape. Polymer melt viscoelasticity, in particular, is an extremely important property of polymeric liquids, since it governs their processability, i.e., their ability to be transformed to final products as a result of the application of a flow field. Understanding the relaxation mechanisms and phenomena occurring at multiple length and time scales in polymers is prerequisite for the development of reliable expressions (namely constitutive laws) describing the relationship between macroscopic flow dynamics and imposed flow kinematics. Such constitutive laws are needed in a number of everyday life applications in relation with (e.g.) the plastics manufacture, the performance of lubricants, the processing of foodstuffs, the dynamics of biological molecules, and many others. To this direction, in addition to experiments and theories, molecular simulations can play a significant role by providing directly the link to molecular-level characteristics of chains. They can address very important questions such as the chain length dependence of the zero shear rate viscosity and its connections to the chemical structure and molecular architecture of the particular polymer, how fine details of molecular architecture affect the response to an imposed shear or elongational flow field, what is the role of branches and polydispersity on polymer dynamics and polymer melt flow, and many others. They can also help validate theories of polymer dynamics and their underlying assumptions. For example, they can provide direct proof for the effective reptation motion invoked by almost all tube models today in explaining the dynamics of entangled polymers. In the last two-three decades significant progress has been made in all these directions. It is the purpose of this article to review what we have learnt about polymer melt viscoelasticity from molecular simulations, with an emphasis on methods employing atomistic models for which there is an immediate connection to the principles of Statistical Mechanics, thus avoiding going through highly complicated mathematical constructions associated with projection operations or the implementation of coarse-graining techniques to less detailed models. Given that the ultimate objective is to use the information provided by molecular simulations to validate or improve known theories and stress/rate-of-strain constitutive equations, a good part of the article is devoted to discussing how atomistic simulation data can be mapped onto theoretical models such as the Rouse, the reptation, and the conformation-tensor based differential viscoelastic equations. This is done in Section 2 of this article. Section 3 discusses the equations of Statistical Mechanics and principles of other fundamental sciences such as Physical Chemistry needed to extract predictions for certain observables from the trajectories of atomistic simulations. We put the emphasis here on properties or material functions which are directly related to polymer melt viscoelasticity, such as (e.g.) the zero shear rate viscosity, the full viscosity curve, the monomer friction factor, the shear modulus of relaxation, the effective tube diameter of the tube model, and the entanglement spacing. In Section 3 we also present representative results for these properties in comparison with available and well-established experimental data. We conclude with Section 4 discussing current efforts and future directions.

2. MOLECULAR MODELLING OF VISCOELASTICITY

2.1. Mapping onto the Rouse model

2.1.1. *Equilibrium Dynamics*

The Rouse model^{1,2} describes the general features of the dynamics of unentangled polymers by assuming only localized interactions. It envisions a polymer as a set of N beads connected along a chain, whose dynamics is described by the Brownian motion of coupled oscillators. Excluded volume effects and hydrodynamic interactions are disregarded, the mobility tensor is considered to be isotropic and the interaction potential is the sum of the harmonic potentials for the springs connecting successive beads. The distribution of random forces on the beads from their environment (the sea of the rest of beads) is also taken to be Gaussian. There are two solutions of the Rouse model, the discrete and the continuous; their predictions agree on long time scales but not on short time scales. If $(\mathbf{R}_1, \mathbf{R}_2, \dots, \mathbf{R}_N) = \{\mathbf{R}_n\}$ are the positions of the N beads, the Rouse model is formulated in terms of the normal coordinates or modes \mathbf{X}_p with $p = 0, 1, 2, \dots, N-1$, each capable of independent motion, defined by:²

$$\mathbf{X}_p = \sum_{n=1}^N \Omega_{np} \mathbf{R}_{n-1}, \Omega_{np} = \sqrt{\frac{2-\delta_{p0}}{N}} \cos\left(\frac{(n-1/2)p\pi}{N}\right) \quad (1)$$

where $\delta_{\alpha\beta}$ is Kronecker's delta. The normal coordinates \mathbf{X}_p with $p>0$ represent the internal conformation of the polymer while the coordinate \mathbf{X}_0 represents the position of the center of mass of the chain, $\mathbf{R}_{cm} \equiv \frac{1}{N} \int_0^N \mathbf{R}_n dn$, whose mean square displacement defines the self diffusion constant D . The expression for the time correlation functions of the normal coordinates \mathbf{X}_p with $p>0$ in the Rouse model is:

$$\langle \mathbf{X}_p(t) \cdot \mathbf{X}_p(0) \rangle = 3 \frac{k_B T}{k_p} \exp\left(-\frac{t}{\tau_p}\right) \quad (2)$$

where

$$k_p = \frac{6\pi^2 k_B T}{\langle R^2 \rangle} p^2 \quad (3a)$$

$$\tau_p = \frac{\tau_1}{p^2}, \text{ and} \quad (3b)$$

$$\tau_1 \equiv \tau_R = \frac{\zeta N^2 b^2}{3\pi^2 k_B T} \quad (3c)$$

The set of characteristic times $\tau_p, p = 1, 2, \dots$, is known as the spectrum of relaxation times, τ_1 is the longest (or the Rouse, τ_R) relaxation time, ζ the monomer friction coefficient, and b the effective bond length so that the equilibrium mean-square chain end-to-end distance is given by $\langle R^2 \rangle_0 = Nb^2$. The corresponding expression for the self diffusion constant D is:

$$D = \frac{k_B T}{N \zeta} \quad (4)$$

Equation (3c) for the longest relaxation time is one of the most significant results of the Rouse model since it enters the expressions for almost all linear viscoelastic properties of unentangled polymers. It defines the:

- relaxation modulus through $G(t) = \frac{c}{N} k_B T \sum_{p=1}^{\infty} \exp \left[-\frac{2p^2 t}{\tau_R} \right]$ (5a)

- zero shear rate viscosity through $\eta_0 = \int_0^{\infty} G(t) dt = \frac{\pi^2}{12} \left(\frac{ck_B T}{N} \right) \tau_R$, and (5b)

- steady-state compliance through $J_e^{(0)} = \frac{1}{\eta_0^2} \int_0^{\infty} t G(t) dt = \frac{2}{5} \frac{N}{ck_B T}$. (5c)

The Rouse model leads also to a number of very useful, closed-form expressions for the mean square displacement (msd) of chain segments $\phi(n, t) \equiv \langle (\mathbf{R}(n, t) - \mathbf{R}(n, 0))^2 \rangle$, and the single-chain intermediate dynamic structure factor $S(q, t)$, a quantity which is experimentally accessible by neutron scattering experimental techniques.³

2.1.2. Calculation of the stress tensor

According to the Rouse model,² the stress tensor is expressed in terms of the normal coordinates as:

$$\sigma_{\alpha\beta}(t) = \frac{N_{ch}}{V} \sum_{p=1}^N k_p \langle X_{p\alpha}(t) X_{p\beta}(t) \rangle \quad (6)$$

where $\langle X_{p\alpha}(t) X_{p\beta}(t) \rangle$ is obtained from the solution to the following time evolution equation:

$$\begin{aligned} \frac{\partial}{\partial t} \langle X_{p\alpha}(t) X_{p\beta}(t) \rangle &= \frac{1}{\zeta_p} \left[2k_p T \delta_{\alpha\beta} - 2k_p \langle X_{p\alpha}(t) X_{p\beta}(t) \rangle \right] \\ &+ \kappa_{\alpha\mu}(t) \langle X_{p\mu}(t) X_{p\beta}(t) \rangle + \kappa_{\beta\mu}(t) \langle X_{p\mu}(t) X_{p\alpha}(t) \rangle \end{aligned} \quad (7)$$

with $\zeta_p = k_p \tau_p$

In this equation, $\boldsymbol{\kappa}(t)$ denotes the applied velocity gradient defined such that the local velocity field is given by $\mathbf{u}(\mathbf{r}, t) = \boldsymbol{\kappa}(t) \cdot \mathbf{r}$. For the case of steady-state uniaxial elongational flow, for example, characterized by the kinematics $u_x = \dot{\epsilon}_{xx}x$, $u_y = \dot{\epsilon}_{yy}y = -\frac{1}{2}\dot{\epsilon}_{xx}y$, and $u_z = \dot{\epsilon}_{zz}z = -\frac{1}{2}\dot{\epsilon}_{xx}z$, one can easily solve for the three non-zero components $\langle X_{px}(t)X_{px}(t) \rangle$, $\langle X_{py}(t)X_{py}(t) \rangle$, and $\langle X_{pz}(t)X_{pz}(t) \rangle$ using the initial condition that at $t=0$, $\langle X_{p\alpha}(t)X_{p\beta}(t) \rangle = \delta_{\alpha\beta} \frac{k_B T}{k_p}$, to get:

$$\langle X_{px}(t)X_{px}(t) \rangle = \frac{k_B T}{k_p} \left\{ B_{p,xx} + (1 - B_{p,xx}) \exp \left[-\frac{2t}{\tau_p B_{p,xx}} \right] \right\} \quad (8a)$$

$$\langle X_{py}(t)X_{py}(t) \rangle = \frac{k_B T}{k_p} \left\{ B_{p,yy} + (1 - B_{p,yy}) \exp \left[-\frac{2t}{\tau_p B_{p,yy}} \right] \right\} \quad (8b)$$

$$\langle X_{pz}(t)X_{pz}(t) \rangle = \frac{k_B T}{k_p} \left\{ B_{p,zz} + (1 - B_{p,zz}) \exp \left[-\frac{2t}{\tau_p B_{p,zz}} \right] \right\} \quad (8c)$$

with $B_{p,xx} = \frac{1}{1 - \tau_p \dot{\epsilon}_{xx}}$, $B_{p,yy} = \frac{1}{1 - \tau_p \dot{\epsilon}_{p,yy}} = \frac{1}{1 + \frac{1}{2} \tau_p \dot{\epsilon}_{xx}}$, and

$$B_{p,zz} = \frac{1}{1 - \tau_p \dot{\epsilon}_{zz}} = \frac{1}{1 + \frac{1}{2} \tau_p \dot{\epsilon}_{p,xx}}.$$

The limiting or steady-state values (i.e., for $t = \infty$) of these expressions are:

$$\langle X_{px}(t)X_{px}(t) \rangle = B_{p,xx} \frac{k_B T}{k_p} \quad (9a)$$

$$\langle X_{py}(t)X_{py}(t) \rangle = B_{p,yy} \frac{k_B T}{k_p} \quad (9b)$$

$$\langle X_{pz}(t)X_{pz}(t) \rangle = B_{p,zz} \frac{k_B T}{k_p}. \quad (9c)$$

In addition to providing a theoretical framework of polymer melt viscoelasticity for unentangled systems, the above results are also very useful in mapping simulation data obtained by extending Monte Carlo methods to beyond-equilibrium conditions by introducing in the Metropolis acceptance criterion an extra term involving a characteristic tensorial parameter associated with the velocity gradient tensor $\boldsymbol{\kappa}$. An example is reviewed in Section 2.3.2 below where a new method (termed GENERIC Monte Carlo) is introduced capable of generating a flow in a polymer melt guided by principles of non-equilibrium thermodynamics.

2.1.3. Stress relaxation

Solutions to the time evolution equation (7) above can also be used to map simulation MD data for the stress relaxation of representative polymer pre-oriented or strained configurations sampled through non-dynamic techniques (such as GENERIC Monte Carlo) not facing the problem of long relaxation times plaguing dynamic methods. The way the strained configurations are generated is a subtle one and requires information from non-equilibrium Statistical Mechanics. Then, once these have been accumulated, one can switch off the thermodynamic field that caused chain deformation, to monitor the relaxation of the system back towards its field-free, equilibrium state. The simulation in this case is performed in a suitable statistical ensemble such as (e.g.) the $NTL_{x\sigma_{yy}\sigma_{zz}}$ introduced by Yang et al.⁴ The relaxation of the system is quantified by monitoring the time evolution of the normal stress in the x -direction (the direction of stretching) keeping the length of the simulation box in the same direction constant, and of certain descriptors of the short- and long-length scale conformation of the polymer chains. In particular, in these MD simulations, one can monitor the temporal evolution of the three diagonal components $\langle X_{px}(t)X_{px}(t) \rangle$, $\langle X_{py}(t)X_{py}(t) \rangle$, and $\langle X_{pz}(t)X_{pz}(t) \rangle$ and map the results onto the corresponding analytical equation of the Rouse model. $\langle \mathbf{X}_p(t)\mathbf{X}_p(t) \rangle$ in this case obeys a Smoluchowski equation of the form of eq. (7) discussed above with the value of the velocity gradient tensor $\boldsymbol{\kappa}$ taken now to be zero and with initial condition for $\langle \mathbf{X}_p(t)\mathbf{X}_p(t) \rangle$ the value calculated at the end of the previous stage [i.e., at the end of the GENERIC Monte Carlo simulation] as given by eq. (9). The result is:

$$\langle X_{px}(t)X_{px}(t) \rangle = \frac{k_B T}{k_p} \left[1 + (B_{p,xx} - 1) \exp\left(-\frac{2t}{\tau_p}\right) \right] \quad (10a)$$

$$\langle X_{py}(t)X_{py}(t) \rangle = \frac{k_B T}{k_p} \left[1 + (B_{p,yy} - 1) \exp\left(-\frac{2t}{\tau_p}\right) \right] \quad (10b)$$

$$\langle X_{pz}(t)X_{pz}(t) \rangle = \frac{k_B T}{k_p} \left[1 + (B_{p,zz} - 1) \exp\left(-\frac{2t}{\tau_p}\right) \right] \quad (10c)$$

The corresponding expressions for the relaxation of the diagonal components σ_{xx} , σ_{yy} , and σ_{zz} of the stress tensor are obtained by substituting expressions (10) into eq. (6):

$$\frac{\sigma_{xx}(t) - \sigma_{xx}(\infty)}{\sigma_{xx}(0) - \sigma_{xx}(\infty)} = \frac{\sum_{p:\text{all}} (B_{p,xx} - 1) \exp\left(-\frac{2t}{\tau_p}\right)}{\sum_{p:\text{all}} (B_{p,xx} - 1)} \quad (11a)$$

$$\frac{\sigma_{yy}(t) - \sigma_{yy}(\infty)}{\sigma_{yy}(0) - \sigma_{yy}(\infty)} = \frac{\sum_{p:\text{all}} (B_{p,yy} - 1) \exp\left(-\frac{2t}{\tau_p}\right)}{\sum_{p:\text{all}} (B_{p,yy} - 1)} \quad (11b)$$

$$\frac{\sigma_{zz}(t) - \sigma_{zz}(\infty)}{\sigma_{zz}(0) - \sigma_{zz}(\infty)} = \frac{\sum_{p:\text{all}} (B_{p,zz} - 1) \exp\left(-\frac{2t}{\tau_p}\right)}{\sum_{p:\text{all}} (B_{p,zz} - 1)} \quad (11c)$$

where $\sum_{p:\text{all}}$ denotes summation over all positive integer numbers p , $\sigma(0)$ is the value of σ at $t=0$ (i.e., at the end of the applied steady-state elongational field or, equivalently, at the beginning of the relaxation process), and $\sigma(\infty)$ the value of σ at infinite time (when the stress has full relaxed), equal to $-P_{\text{ext}}\delta$, where δ is the unit tensor.

The Rouse model provides also an analytical expression for the relaxation of the xx component of the scaled conformation tensor $\tilde{\mathbf{c}} \equiv \frac{\langle \mathbf{RR} \rangle}{3\langle R^2 \rangle_0}$, by using that $\tilde{\mathbf{c}}(t) = \frac{3}{\langle R^2 \rangle_0} \sum_{p:\text{odd}} 16 \langle \mathbf{X}_p(t) \mathbf{X}_p(t) \rangle$, where $\langle R^2 \rangle_0$ denotes the average chain end-to-end distance at equilibrium. The result is:

$$\frac{\tilde{c}_{xx}(t) - \tilde{c}_{xx}(\infty)}{\tilde{c}_{xx}(0) - \tilde{c}_{xx}(\infty)} = \frac{\sum_{p:\text{odd}} \frac{1}{k_p} (B_{p,xx} - 1) \exp\left(-\frac{2t}{\tau_p}\right)}{\sum_{p:\text{odd}} \frac{1}{k_p} (B_{p,xx} - 1)} \quad (12a)$$

$$\frac{\tilde{c}_{yy}(t) - \tilde{c}_{yy}(\infty)}{\tilde{c}_{yy}(0) - \tilde{c}_{yy}(\infty)} = \frac{\sum_{p:\text{odd}} \frac{1}{k_p} (B_{p,yy} - 1) \exp\left(-\frac{2t}{\tau_p}\right)}{\sum_{p:\text{odd}} \frac{1}{k_p} (B_{p,yy} - 1)} \quad (12b)$$

$$\frac{\tilde{c}_{zz}(t) - \tilde{c}_{zz}(\infty)}{\tilde{c}_{zz}(0) - \tilde{c}_{zz}(\infty)} = \frac{\sum_{p:\text{odd}} \frac{1}{k_p} (B_{p,zz} - 1) \exp\left(-\frac{2t}{\tau_p}\right)}{\sum_{p:\text{odd}} \frac{1}{k_p} (B_{p,zz} - 1)} \quad (12c)$$

where $\sum_{p:\text{odd}}$ denotes summation over all odd positive integer numbers p , $\tilde{\mathbf{c}}(0)$ is the value of $\tilde{\mathbf{c}}$ at time $t=0$ (i.e., at the end of the applied steady-state elongational field or,

equivalently, at the beginning of the relaxation process) and $\bar{\mathbf{c}}(\infty)$ the value of $\bar{\mathbf{c}}$ at infinite time (when the polymer chain conformations have fully relaxed), equal to $\bar{\mathbf{d}}$. From a practical point of view, eq. (12) for the relaxation of $\bar{\mathbf{c}}$ is a more suitable expression to use than eq. (11) for the relaxation of $\boldsymbol{\sigma}$ in order to map the simulation data onto the Rouse model, because the conformation tensor is calculated with a higher accuracy than the stress tensor in molecular simulations.

2.2. Mapping onto the equilibrium dynamics of the reptation model

For polymer melts of high molecular weight, polymer dynamics becomes extremely complicated due to topological constraints arising from chain connectivity and the fact that polymers cannot cross each other. As discussed by Doi-Edwards,² this interaction is singular since there is no parameter describing its strength. Its effect is null for the static properties but quite serious for the dynamic properties. Thus, although experimental results on the viscoelasticity of high molecular weight (MW) polymers appeared quite early (since the 50's), a successful theoretical explanation was offered only much later by the effective tube model of the reptation theory. The model, originally proposed to describe the problem of rubber elasticity, considers that the intrinsic properties of the chain are still represented by the Rouse model consisting of N segments with bond length b and friction constant ζ ; their dynamics, however, is significantly affected by the topological constraints due to mutual entanglements with surrounding chains which restrict the number of allowed conformations compared to that in free space. The allowed chain conformations are effectively confined in a tube-like region whose axis is defined by the shortest path connecting the two ends of the chain having the same topology with the chain itself relative to the constraints. Such a path is called the primitive path and can move back and forth only along its contour. Its dynamics is characterized by the following assumptions:^{5-8,2}

- a) A point on the primitive path is denoted by the contour length s measured from the chain end. It is called the primitive chain segment s and its position at time t is defined by the unit vector tangent to the primitive chain at s :

$$\mathbf{u}(s, t) = \frac{\partial}{\partial s} \mathbf{R}(s, t) \quad (13)$$

The correlation of tangent vectors $\mathbf{u}(s, t)$ and $\mathbf{u}(s', t)$ decreases quickly with $|s - s'|$, implying a Gaussian conformation for the primitive chain on a large length scale. Given that the mean-square distance between two points on a Gaussian chain is proportional to their separation along the chain contour, it is concluded that:

$$\left\langle (\mathbf{R}(s, t) - \mathbf{R}(s', t))^2 \right\rangle = \alpha |s - s'| \quad (14)$$

where the new parameter α introduced by the model is called the step length of the primitive chain.

- b) The contour length L of the primitive chain is constant and is described by the following expression:

$$L = \frac{\langle R^2 \rangle_0}{\alpha} = \frac{Nb^2}{\alpha} \quad (15)$$

implying that the theory neglects contour length fluctuations.

c) The primitive chain can move back and forth only along itself with a certain diffusion constant D_c , which is identified as the diffusion constant of the Rouse model:

$$D_c = \frac{k_B T}{N \zeta} \quad (16)$$

since the motion of the primitive chain corresponds to the overall translation of the Rouse chain along the tube.

d) The theory does not answer the question of what diameter should be assigned to the tube: it only considers it to be determined by local conditions (i.e., not to depend on the length of the chain), and practically to be proportional to the step length α of the primitive chain.

Clearly, the theory as presented initially with the above assumptions addresses only the dynamics of a single chain in a fixed network. In real systems (concentrated polymer solutions and melts of high MW polymers), additional mechanisms involving the collective motion of chains (such as constraint release, tube renewal, etc.) will also be very important. We discuss many of the consequences of these mechanisms in the subsequent sections of this Review.

Key in the reptation theory is the function $\psi(s, t)$ representing the probability that the original tube segment s is remaining at time t , which is equivalent to the probability that the primitive chain segment s is in the original tube (the tube specified for the primitive chain at time $t=0$). For linear polymers in a fixed network, implying that contour length fluctuation (CLF) effects and constraint-release (CR) mechanisms are neglected, this function obeys a diffusion equation whose solution is:²

$$\psi(s, t) = \sum_{p:odd} \frac{4}{p\pi} \sin\left(\frac{p\pi s}{L}\right) \exp\left(-\frac{p^2 t}{\tau_d}\right) \quad (17)$$

where τ_d is the reptation or disentanglement time (the time needed for the primitive chain to disengage from the tube it was confined to at $t=0$). The function $\psi(s, t)$ is central in the Doi-Edwards theory since it defines all linear viscoelastic properties of the polymer [see Ref. 2]. It defines:

- the spectrum of relaxation times, and consequently the disentanglement time τ_d , through:

$$\int_0^L \psi(s, t) ds = L \sum_{p:odd} \frac{8}{p^2 \pi^2} \exp\left(-\frac{p^2 t}{\tau_d}\right) \quad (18a)$$

- the relaxation modulus of the polymer through:

$$G(t) = G_N^0 \frac{1}{L} \int_0^L \psi(s,t) ds \quad (18b)$$

- the storage and loss moduli through:

$$G'(\omega) = \omega \int_0^{\infty} G(t) \sin(\omega t) dt, \quad G''(\omega) = \omega \int_0^{\infty} G(t) \cos(\omega t) dt \quad (18c)$$

- the zero shear viscosity through:

$$\eta_0 = G_N^0 \frac{1}{L} \int_0^{\infty} \int_0^L \psi(s,t) ds dt = \int_0^{\infty} G(t) dt \quad (18d)$$

- the steady-state compliance through:

$$J_e^{(0)} = \frac{\int_0^{\infty} t G(t) dt}{\left[\int_0^{\infty} t G(t) dt \right]^2} \quad (18e)$$

For the particular case the function $\psi(s,t)$ is given by eq. (17) of the Doi-Edwards theory (implying that CLF and CR mechanisms are neglected⁹⁻¹³), the resulting expressions for the zero shear rate viscosity and the chain center-of-mass self-diffusion coefficient central in the Doi-Edwards theory assume the following forms:

$$\eta_0 = \frac{\pi^2}{12} G_N^0 \tau_d \quad (18f)$$

and

$$D = \frac{D_c}{3Z} \quad (18g)$$

where Z denotes the number of entanglements per chain.

Of interest in the reptation theory is also the segmental dynamics as quantified by the mean-square displacement (msd) $\phi_n(t) = \left\langle \left(\mathbf{R}_n(t) - \mathbf{R}_n(0) \right)^2 \right\rangle$ of the Rouse segments n up to time t , where $\mathbf{R}_n(t)$ is the position vector of segment n at time t . Although the exact analytical calculation of $\phi_n(t)$ is impossible, Doi-Edwards analyzed its basic features in a very detailed way and concluded that a typical $\phi_n(t)$ - vs.- t plot for entangled melts should exhibit in general four distinct regions corresponding to three characteristic times: the time τ_e denoting the onset of topological constraints (entanglements) to the diffusive motion of the segments, the Rouse time τ_R , and the disentanglement time τ_d . For times t such that $t < \tau_e$, a Rouse segment executes anomalous diffusion in free space (ballistic motion), and thus $\phi_n(t) \sim t^{1/2}$. For times t such that $\tau_e < t < \tau_R$, the motion of the segment perpendicular to the

primitive path is restricted while that along the path itself remains free, implying a behavior which is a consequence of two effects: the Rouse-like motion of the segment and the tube constraints, and thus $\phi_n(t) \sim t^{1/4}$. For times t such that $\tau_R < t < \tau_d$, segmental dynamics is identical to that predicted by the primitive chain dynamics and $\phi_n(t) \sim t^{1/2}$. Finally, for times t such that $t > \tau_d$, the dynamics is governed by the reptation process, the segments enter the regime of Fickian diffusion, and thus $\phi_n(t) \sim t$. The four scaling laws are represented as follows:

$$\phi_n(t) \propto \begin{cases} t^{1/2} & t \leq \tau_e \\ t^{1/4} & \tau_e \leq t \leq \tau_R \\ t^{1/2} & \tau_R \leq t \leq \tau_d \\ t^1 & \tau_d \leq t \end{cases} \quad (19)$$

As we will see in Section 3.2 below, all these characteristic scalings have been observed in MD simulations with model linear polymer melts such as polyethylene (PE) and *cis*-1,4 and *trans*-1,4-polybutadiene (PB), but also with H-shaped polymers, with scaling exponents remarkably close to those derived by the theory.

2.3. Mapping onto differential constitutive viscoelastic models

In addition to the Rouse and reptation theories of polymer dynamics, a family of models that is widely used to describe polymer melt viscoelasticity is that of the differential, non-separable equations based on the concept of the conformation tensor, such as the Phan-Thien/Tanner (PTT)^{14,15} and the Giesekus¹⁶ viscoelastic models based on network theories. Written in terms of the extra stress tensor $\boldsymbol{\tau}$ (i.e., the polymer contribution to the stress), the two constitutive models read:

$$\lambda_0 \dot{\boldsymbol{\tau}}_{[1]} + \boldsymbol{\tau} + \frac{\beta}{nk_B T} \boldsymbol{\tau} \cdot \boldsymbol{\tau} = \eta_0 \dot{\boldsymbol{\gamma}} \quad (\text{Giesekus model}) \quad (20)$$

and

$$\lambda_0 \dot{\boldsymbol{\tau}}_{[1]} + \exp\left[\frac{\varepsilon}{nk_B T} \text{tr} \boldsymbol{\tau}\right] \boldsymbol{\tau} = \eta_0 \dot{\boldsymbol{\gamma}} \quad (\text{PTT model}) \quad (21)$$

respectively. In the above expressions, the subscript [1] denotes the upper-convected Maxwell derivative defined as:

$$\dot{\boldsymbol{\tau}}_{[1]} \equiv \frac{\partial \boldsymbol{\tau}}{\partial t} + \mathbf{u} \cdot \nabla \boldsymbol{\tau} - \boldsymbol{\tau} \cdot \nabla \mathbf{u} - (\nabla \mathbf{u})^T \cdot \boldsymbol{\tau} \quad (22)$$

where λ_0 is a characteristic relaxation time, η_0 a characteristic viscosity, β denotes the Giesekus parameter, ε a numerical constant, n the chain number density, k_B Boltzmann's constant, and $\text{tr} \boldsymbol{\tau}$ the trace of the extra stress tensor.

A key feature of the Giesekus model is the postulation of an anisotropic mobility tensor which gives rise to a quadratic term in the constitutive equation, and hence to a non-vanishing value for the second normal stress coefficient. On the other hand, the Giesekus model predicts a monotonic increase with time of the corresponding extensional viscosity in the start-up of any steady extensional flow (uniaxial, biaxial, planar), up to a steady-state value.¹⁷ Also, at large shear rates, it predicts a shear stress that is independent of shear rate. Both of these drawbacks are related to the assumption of a linear (Hookean) spring force law for the underlying dumbbell mechanical model, permitting infinite chain extension. To account for finite extensibility, Wiest¹⁸ and Doufas^{19,20} proposed modifications of the Giesekus model by incorporating in the constitutive equation non-linear elastic effects via the Peterlin closure with Wagner's and Cohen's approximation, respectively.²¹⁻²⁴ Recently, Housiadas and Beris²⁵ discussed another serious limitation of the FENE-P model (the finitely-extensible nonlinear elastic constitutive model with the Peterlin approximation). At high extensional deformations where chains assume practically their fully extended states, the model results in unbounded predictions for the polymer free energy (it becomes infinite), which is inconsistent with the postulate of a purely entropic contribution to the free energy (the entropy based on chain conformation must be finite in polymeric systems with a finite number of degrees of freedom and finite chain extensibility). Housiadas and Beris²⁵ proposed a phenomenological modification of the model so that the nonequilibrium free energy remains always bounded between 0 and a certain maximum value which is a function only of the extensibility parameter of the model; the new model in which no new parameters are introduced (except for the extensibility parameter) was given the name FENE-PB (B for bounded).

Atomistic simulations can tremendously help improve these models by providing a more accurate expression for the free energy of deformation based on the findings of carefully designed Monte Carlo simulations of polymer melt elasticity.²⁶⁻³⁰ Moreover, molecular simulations can define the conditions under which the contribution to free energy is purely entropic or if there exists an additional energetic component due to favorable lateral interactions at high fields as chain segments become more and more oriented. There are two ways through which atomistic simulation results can be mapped onto differential constitutive models such as the Giesekus and the PTT ones. The first is to execute direct non-equilibrium molecular dynamics simulations (NEMD)³¹ to calculate the conformation and stress tensor components and then to compare against the predictions of the differential model for the given value of the rate-of-strain tensor. The second (GENERIC Monte Carlo)²⁶⁻³⁰ employs Monte Carlo in an expanded statistical ensemble (i.e., an ensemble where additional synthetic nonequilibrium thermodynamic force fields are included) capable of driving a model system to statistically appropriate nonequilibrium phase-space points corresponding to the imposed external field. The two methods are discussed below.

2.3.1. The Non-Equilibrium Molecular Dynamics Method

The first algorithm for the simulation of a system under an applied flow field was the DOLLS algorithm proposed by Hoover et al.³² If $\mathbf{\nabla}\mathbf{u}$ is the applied velocity gradient tensor, the DOLLS algorithm starts with the following expression for the Hamiltonian:

$$H(\mathbf{p}, \mathbf{q}) = \sum_{i=1}^N \frac{p_i^2}{2m_i} + U^{pot}(\mathbf{q}) + \sum_{i=1}^N \mathbf{q}_i \mathbf{p}_i : (\nabla \mathbf{u})^T \quad (23)$$

and generates the following set of canonical equations of motion:

$$\begin{aligned} \dot{\mathbf{q}}_i &= \frac{\partial H}{\partial \mathbf{p}_i} = \frac{\mathbf{p}_i}{m_i} + \mathbf{q}_i \cdot \nabla \mathbf{u} \\ \dot{\mathbf{p}}_i &= -\frac{\partial H}{\partial \mathbf{q}_i} = \mathbf{F}_i - \nabla \mathbf{u} \cdot \mathbf{p}_i \end{aligned} \quad (24)$$

where $\mathbf{F}_i = -\frac{\partial U^{pot}}{\partial \mathbf{q}_i}$. In the above equations, \mathbf{q}_i and \mathbf{p}_i are the vectors of generalized momentum and generalized position of particle i with mass m_i .

Although DOLLS is derived by a Hamiltonian and generates canonical equations of motion, it results in an incorrect prediction for the shear flow at high values of shear rate. The second and most widely used algorithm for NEMD simulations has been proposed by Evans and Morriss and it is the SLLOD algorithm.³³⁻³⁴ This algorithm is not generated by a Hamiltonian. Its equations of motion are:

$$\begin{aligned} \dot{\mathbf{q}}_i &= \frac{\mathbf{p}_i}{m_i} + \mathbf{q}_i \cdot \nabla \mathbf{u} \\ \dot{\mathbf{p}}_i &= \mathbf{F}_i - \mathbf{p}_i \cdot \nabla \mathbf{u} \end{aligned} \quad (25)$$

For flows such that $(\nabla \mathbf{u}) = (\nabla \mathbf{u})^T$, these equations are identical to those proposed by the DOLLS algorithm. As reported by Tuckerman et al.,³⁵ a drawback of the SLLOD algorithm is that it does not satisfy Newton's equations of motion, namely, $m_i \ddot{\mathbf{q}}_i = \mathbf{F}_i$. Indeed, from eqs. (25) it can be shown that:

$$m_i \ddot{\mathbf{q}}_i = \mathbf{F}_i + m_i \mathbf{q}_i \cdot \nabla \mathbf{u} \cdot \nabla \mathbf{u} \quad (26)$$

which is inconsistent with Newton's law except for the case of the simple shear flow for which the last term on the rhs of eq. (26) disappears. Thus, the application of SLLOD to NEMD simulations of polymer has been practically limited to systems subjected to shear,³⁶ where also one makes use of the Lees-Edwards boundary conditions.³⁷

Although shear can be easily simulated using the Lees-Edwards boundary conditions, extensional flows (uniaxial, biaxial, and planar) are notoriously difficult to follow for sufficient time. This happens because in these flows the fluid is continuously stretched in at least one direction, and continuously compressed in at least another. As a result of the latter, the lifetime of the NEMD simulation is rather short since very quickly at least one of the dimensions of the simulation cell becomes smaller than the minimum allowed length (which is twice the range of the interaction potential). For polymers, in particular, with long relaxation times, this implies that the simulation will have to be stopped before the system reaches the steady state for the

given (applied) deformation gradient. The problem has been solved today only for the case of planar elongational flow by Kraynik and Reinelt.³⁸ Let us consider a fluid subjected to planar elongational flow with x being the direction of expansion with a strain rate $\dot{\epsilon}$, y the direction of contraction with a strain rate $-\dot{\epsilon}$, and z the neutral direction. We consider also a square lattice on the xy plane, which at time $t=0$ is oriented with respect to the direction of elongation by an angle θ . Kraynik and Reinelt proved algebraically that for certain discrete values of the angle θ and for certain discrete values of the Hencky strain defined as $\epsilon_p = \dot{\epsilon}t_p$ where t_p is the lattice strain period and only for them, such a lattice is spatially and temporally periodic, allowing a conventional NEMD simulation to run for theoretically infinite simulation times. The simulation cell, which should be initially oriented at certain discrete angles with respect to the direction of elongation, will in this case be both spatially and temporally periodic and its boundaries will evolve in time consistently with the applied strain rate.

By combining the SLLOD algorithm (even if it does not satisfy the Newton's law in extensional flows) with Kraynik and Reinelt's idea of temporal and spatial periodicity of lattice vectors in planar extensional flow, NEMD simulations of short polymers subjected to PEF have been reported.³⁹⁻⁴⁰ A significant problem mentioned in these simulations is that they are inherently unstable over long simulation times. This is caused by an exponential growth of the total linear momentum in the contracting direction, which leads eventually to an aphysical phase transition in the flow. Tuckerman et al.³⁵ showed that in the absence of time dependent boundary conditions, there exists a conserved energy for the SLLOD equations of motion which can be used to carry out an analysis of the phase space generated by them. The analysis predicted a linear velocity profile for the case of planar Couette flow, a finding which implies that the resultant flow is field-driven rather than boundary-driven. Tuckerman et al.³⁵ also noticed that the conserved energy quantity does not generate a distribution that is canonical in the positions for time independent boundary conditions. Thus, they proposed a generalization of the SLLOD algorithm, G-SLLOD, that correctly generates a distribution function which is canonical in the laboratory velocities and positions for a general strain rate. The G-SLLOD equations of motion with a Nosé-Hoover thermostat have the following form:

$$\begin{aligned}
 \dot{\mathbf{q}}_i &= \frac{\mathbf{p}_i}{m_i} + \mathbf{q}_i \cdot \nabla \mathbf{u} \\
 \dot{\mathbf{p}}_i &= \mathbf{F}_i - \mathbf{p}_i \cdot \nabla \mathbf{u} - m_i \mathbf{q}_i \cdot \nabla \mathbf{u} \cdot \nabla \mathbf{u} - \frac{p_\eta}{Q} \mathbf{p}_i \\
 \dot{\eta} &= \frac{p_\eta}{Q} \\
 \dot{p}_\eta &= \sum_{i=1}^N \frac{\mathbf{p}_i^2}{m_i} - dNk_B T
 \end{aligned}
 \tag{27}$$

where η is the thermostat variable, p_η its momentum and Q its effective mass, and where d denotes the space dimensionality.

According to Edwards and collaborators,⁴¹⁻⁴³ the unphysical exponential growth of the total linear momentum in PEF simulations with the SLLOD algorithm has its origins to two sources, to the SLLOD algorithm itself and to way the Kraynik and Reinelt boundary conditions are implemented. Thus Edwards et al.⁴¹⁻⁴³ proposed the p-SLLOD algorithm (p for proper) which removes the first source and together with an appropriate implementation of the Kraynik and Reinelt boundary conditions can be used in NEMD simulations of PEF without encountering the aphysical phenomenon reported by Todd and Daivis.³⁹ Edwards et al.⁴¹⁻⁴³ distinguished between the laboratory velocity \mathbf{v}_i of atom i (the velocity with respect to a fixed frame of reference) and the peculiar velocity $\dot{\mathbf{v}}_i$ (the velocity relative to the externally imposed flow velocity \mathbf{u}). The corresponding momenta are denoted as \mathbf{p}_i and $\dot{\mathbf{p}}_i$. The corresponding sets (\mathbf{p}, \mathbf{q}) and $(\dot{\mathbf{p}}, \dot{\mathbf{q}})$ of generalized coordinates are related through:

$$\begin{aligned}\dot{\mathbf{p}}_i &= \mathbf{p}_i + m_i \mathbf{q}_i \cdot \nabla \mathbf{u} \\ \dot{\mathbf{q}}_i &= \mathbf{q}_i\end{aligned}\tag{28}$$

Then, Edwards et al.⁴¹⁻⁴³ write the Hamiltonian of the system as:

$$H'(\dot{\mathbf{p}}, \dot{\mathbf{q}}) = \sum_{i=1}^N \frac{1}{2m_i} \dot{\mathbf{p}}_i'^2 + U^{pot}(\dot{\mathbf{q}})\tag{29}$$

from which the following canonical equations of motion are derived:

$$\begin{aligned}\dot{\mathbf{q}}_i &= \frac{\partial H'}{\partial \dot{\mathbf{p}}_i} = \frac{\dot{\mathbf{p}}_i}{m_i} \\ \dot{\mathbf{p}}_i &= -\frac{\partial H'}{\partial \dot{\mathbf{q}}_i} = \mathbf{F}_i\end{aligned}\tag{30}$$

or, equivalently, in the (\mathbf{p}, \mathbf{q}) space:

$$\begin{aligned}\dot{\mathbf{q}}_i &= \frac{\mathbf{p}_i}{m_i} + \mathbf{q}_i \cdot \nabla \mathbf{u} \\ \dot{\mathbf{p}}_i &= \mathbf{F}_i - \mathbf{p}_i \cdot \nabla \mathbf{u} - m_i \mathbf{q}_i \cdot \nabla \mathbf{u} \cdot \nabla \mathbf{u}\end{aligned}\tag{31}$$

These equations satisfy Newton's law, namely that $m_i \ddot{\mathbf{q}}_i = \mathbf{F}_i$; also for flows such that $\nabla \mathbf{u} \cdot \nabla \mathbf{u} = 0$, the p-SLLOD algorithm reduces to the SLLOD algorithm. With a Nosé-Hoover thermostat, the p-SLLOD equations of motion take the following final form:

$$\begin{aligned}
 \dot{\mathbf{q}}_i &= \frac{\mathbf{p}_i}{m_i} + \mathbf{q}_i \cdot \nabla \mathbf{u} \\
 \dot{\mathbf{p}}_i &= \mathbf{F}_i - \mathbf{p}_i \cdot \nabla \mathbf{u} - m_i \mathbf{q}_i \cdot \nabla \mathbf{u} \cdot \nabla \mathbf{u} - \frac{p_\eta}{Q} \mathbf{p}_i \\
 \dot{\eta} &= \frac{p_\eta}{Q} \\
 \dot{p}_\eta &= \sum_{i=1}^N \frac{\mathbf{p}_i^2}{m_i} - dNk_B T
 \end{aligned} \tag{32}$$

i.e., they are identical to the equations corresponding to the G-SLLOD algorithm.

2.3.2. The GENERIC Monte Carlo method

The method is founded on the GENERIC (the General Equation for the NonEquilibrium Reversible-Irreversible Coupling) formalism of nonequilibrium thermodynamics and permits the formulation of rigorous MC simulation schemes in generalized statistical ensembles where, in addition to the known thermodynamic fields (e.g., temperature and pressure), extra fields are considered corresponding to certain structural or conformational system properties. Key elements in the new simulation technique, also termed GENERIC MC, are the vector \mathbf{x} of the proper state variables, the vector $\boldsymbol{\lambda}$ of the corresponding conjugate fields, and the relevant probability density function $\rho_{[\boldsymbol{\lambda}]}$ which in the canonical GENERIC ensemble is written as:

$$\rho_{[\boldsymbol{\lambda}]}(\mathbf{z}) = \frac{1}{Q(\boldsymbol{\lambda})} \exp\left(-\sum_k \lambda_k \Pi_k(\mathbf{z})\right); \quad Q(\boldsymbol{\lambda}) = \int \exp\left(-\sum_k \lambda_k \Pi_k(\mathbf{z})\right) d\mathbf{z} \tag{33}$$

Here \mathbf{z} denotes the phase space consisting of the atomistic position and momentum coordinates while λ_k represents the intensive thermodynamic field exciting the conjugate extensive thermodynamic quantity Π_k ; the corresponding thermodynamic state variable x_k is simply the average of Π_k . The total set of state variables \mathbf{x} of the physical system is typically expressed as $\mathbf{x} = \{\rho(\mathbf{r}), \mathbf{M}(\mathbf{r}), \varepsilon(\mathbf{r}), \mathbf{X}(\mathbf{r})\}$, where ρ denotes the mass density, \mathbf{M} the momentum density, ε the internal energy, \mathbf{X} the structural variables characterizing nonequilibrium states, and \mathbf{r} the position vector. In the GENERIC formalism, the Lagrange multipliers λ_k are defined through:

$$\frac{\delta S(\mathbf{x})}{\delta x_k} = k_B \lambda_k \tag{34}$$

where S denotes the entropy. For the family of differential constitutive equations of interest here (such as the upper-convected Maxwell (UCM), the PTT and the Giesekus models), the relevant structural variable \mathbf{X} is the (dimensionless) conformation tensor $\tilde{\mathbf{c}}$ defined as the tensor of the second moment of the distribution function for the chain end-to-end vector normalized by its equilibrium isotropic value.²⁶ According to the generalized bracket⁴⁴ or GENERIC⁴⁵ formalisms of non-equilibrium thermodynamics,

for all of them, the evolution equation has the form of the following generalized differential equation:

$$\dot{\tilde{\mathbf{c}}}_{[1]} = -\mathbf{\Lambda} \cdot \frac{\delta A(\tilde{\mathbf{c}})}{\delta \tilde{\mathbf{c}}} \Leftrightarrow \dot{\tilde{\mathbf{c}}}_{[1]} = -nk_B T \mathbf{\Lambda} \cdot \boldsymbol{\alpha} \quad (35a)$$

$$\boldsymbol{\alpha} \equiv \frac{1}{nk_B T} \frac{\delta A(\tilde{\mathbf{c}})}{\delta \tilde{\mathbf{c}}} \left(= -\frac{\boldsymbol{\lambda}}{n} \right) \quad (35b)$$

$$\boldsymbol{\tau} = 2nk_B T \tilde{\mathbf{c}} \cdot \frac{\delta A(\tilde{\mathbf{c}})}{\delta \tilde{\mathbf{c}}} \quad (35c)$$

where n denotes the chain number density. Equations (35) involve two basic building blocks: the fourth-order relaxation matrix $\mathbf{\Lambda}$ and the free energy A . Typical expressions of $\mathbf{\Lambda}$ and the free energy A reproducing a number of known viscoelastic models are given in Ref. 44. The tensor $\mathbf{\Lambda}$ in particular has the following form:

$$\Lambda_{\alpha\beta\gamma\epsilon}(\tilde{\mathbf{c}}) = f_1(I_1) \left(\tilde{c}_{\alpha\gamma} \delta_{\beta\epsilon} + \tilde{c}_{\alpha\epsilon} \delta_{\beta\gamma} + \tilde{c}_{\beta\gamma} \delta_{\alpha\epsilon} + \tilde{c}_{\beta\epsilon} \delta_{\alpha\gamma} \right) + 2f_2(I_1) \left(\tilde{c}_{\alpha\gamma} \tilde{c}_{\beta\epsilon} + \tilde{c}_{\alpha\epsilon} \tilde{c}_{\beta\gamma} \right) \quad (36)$$

where I_1 represents the first invariant of $\tilde{\mathbf{c}}$ (i.e., the trace of $\tilde{\mathbf{c}}$), δ is the unit tensor, f_1 and f_2 arbitrary functions of I_1 , and the Einstein summation convention has been assumed over repeated Greek indices. Guided from eqs. (35a)-(35c), one can design some very interesting simulations based on the Monte Carlo method (and not on the molecular dynamics one, which suffers from the problem of long relaxation times) provided that a clear kinematic interpretation can be assigned to the Lagrange multipliers $\boldsymbol{\alpha}$ or $\boldsymbol{\lambda}$ ($\boldsymbol{\lambda} = -n\boldsymbol{\alpha}$).²⁸ Unfortunately, as eqs. (35) show, the definition of the Lagrange multiplier(s) and the evolution equation itself suggest different values for $\boldsymbol{\alpha}$ for different viscoelastic models. For example, for the case of simple shear flow described by the kinematics:

$$\nabla \mathbf{u} = \begin{pmatrix} 0 & 0 & 0 \\ \dot{\gamma} & 0 & 0 \\ 0 & 0 & 0 \end{pmatrix}, \quad (37)$$

according to the UCM model:

$$\boldsymbol{\alpha} = \begin{pmatrix} \frac{1}{2} \frac{\lambda_0^2 \dot{\gamma}_0^2}{1 + \lambda_0^2 \dot{\gamma}_0^2} & \frac{1}{2} \frac{\lambda_0 \dot{\gamma}_0}{1 + \lambda_0 \dot{\gamma}_0} & 0 \\ \frac{1}{2} \frac{\lambda_0 \dot{\gamma}_0}{1 + \lambda_0 \dot{\gamma}_0} & -\frac{1}{2} \frac{\lambda_0^2 \dot{\gamma}_0^2}{1 + \lambda_0^2 \dot{\gamma}_0^2} & 0 \\ 0 & 0 & 0 \end{pmatrix} \quad (38)$$

whereas according to the Giesekus model:

$$\boldsymbol{\alpha} = \frac{1}{2} \lambda_0 [\boldsymbol{\delta} + \beta(\tilde{\mathbf{c}} - \boldsymbol{\delta})]^{-1} \cdot [\nabla \mathbf{u} + \tilde{\mathbf{c}}^{-1} \cdot (\nabla \mathbf{u})^T \cdot \tilde{\mathbf{c}}] \quad (39)$$

i.e., $\boldsymbol{\alpha}$ is given in terms of the conformation tensor $\tilde{\mathbf{c}}$ (and the unknown Giesekus parameter β) whose components satisfy the following algebraic equations:

$$\begin{aligned} (1-2\beta)\tilde{c}_{yy} + \beta(\tilde{c}_{xy}^2 + \tilde{c}_{yy}^2) &= 1 - \beta \\ (1-2\beta)\tilde{c}_{xy} - \lambda_0\dot{\gamma}_0\tilde{c}_{xy} + \beta(\tilde{c}_{xx}\tilde{c}_{xy} + \tilde{c}_{xy}\tilde{c}_{yy}) &= 0 \\ (1-2\beta)\tilde{c}_{xx} - 2\lambda_0\dot{\gamma}_0\tilde{c}_{xy} + \beta(\tilde{c}_{xx}^2 + \tilde{c}_{xy}^2) &= 1 - \beta \\ \tilde{c}_{zz} &= 1 \end{aligned} \quad (40)$$

Adhering to any of the two would imply therefore that, for a given pre-specified value of the dimensionless shear rate $\lambda_0\dot{\gamma}_0$ (i.e., of the Deborah number $De = \lambda_0\dot{\gamma}_0$), the phase-points sampled by the GENERIC MC simulation would not be the true non-equilibrium states corresponding to that shear rate but some model-dependent phase-points. To overcome this, Baig and Mavrantzas²⁸ proposed an iterative method of calculating the non-zero components of the tensor $\boldsymbol{\alpha}$, whose most general form for the case of simple shear is:

$$\boldsymbol{\alpha} = \begin{pmatrix} \alpha_{xx} & \alpha_{xy} & 0 \\ \alpha_{xy} & \alpha_{yy} & 0 \\ 0 & 0 & \alpha_{zz} \end{pmatrix} \quad (41)$$

based on independent nonequilibrium molecular dynamics (NEMD) simulations on the same system, for a given value of De . In fact, as noticed by Baig and Mavrantzas, all existing viscoelastic models proposed so far suggest a zero value for the zz component of the tensor $\boldsymbol{\alpha}$, thus, in the GENERIC MC simulations the following form can be assumed for $\boldsymbol{\alpha}$:

$$\boldsymbol{\alpha} = \begin{pmatrix} \alpha_{xx} & \alpha_{xy} & 0 \\ \alpha_{xy} & \alpha_{yy} & 0 \\ 0 & 0 & 0 \end{pmatrix} \quad (42)$$

The new method permits mapping atomistic GENERIC MC simulation data onto eq. (35), the constitutive equation of the family of conformation tensor viscolastic models, with the following advantages: (a) the accurate calculation of the free energy of the deformed melt through thermodynamic integration (which can be used to test analytical expressions widely invoked in the literature), (b) the realization that expression (36) for the relaxation matrix $\boldsymbol{\Lambda}$ generates always a zero value for the zz component of the tensor $\boldsymbol{\alpha}$ (this is particularly important for the predictive capability of these models, since α_{zz} is related with the second normal stress difference), and (c) the possibility to calculate the free energy of deformation of polymer melts.^{46, 47} And then check the assumption of purely entropic elasticity⁴⁸⁻⁵² and the validity of simple linear formulae such as Kramer's expression²⁴ relating stress and conformation tensors, and above all, the possibility to use all this information to improve existing viscoelastic

models or to design new ones with enhanced predictive capability. Stephanou et al.,⁵³ for example, have proposed recently a consistent generalization of the Giesekus model accounting for finite chain extensibility with non-linear molecular stretching, non-affine deformation, and variation of the longest chain relaxation time with chain conformation.

3. RESULTS

In this Section, we will demonstrate the type of information that one can get for the mechanical and rheological properties of polymer melts either directly from molecular simulations or by mapping the information contained in the atomistic MD and MC trajectories onto the equations presented in Section 2. Generally speaking, MD and MC differ from other forms of numerical computation in that the computer with which the calculations are carried out is not merely a machine but the virtual laboratory in which the system is studied. In such a “laboratory”, understanding is achieved by constructing first a theoretical model of molecular behavior able to reproduce and predict experimental observations and solving it using a suitable algorithm or a computer program. The two methods provide exact results to statistical mechanics problems for the given molecular model in preference to approximate solutions.^{54,55} In MD,⁵⁶⁻⁶⁰ the atoms are moved according to the inter- and intramolecular forces derived from the potential function⁶¹⁻⁶⁵ by solving Newton’s equations of motion whereas in MC⁶⁶ one relies on transition probabilities between different states of the simulated system for the given potential model. These transitions are traced through a scheme that involves in general three (3) steps: (a) generation of an initial configuration, (b) trial of a randomly generated system configuration, and (c) evaluation of an “acceptance criterion” for the trial configuration and comparison to a random number to decide whether the trial configuration will be accepted or rejected. The acceptance criterion is usually formulated in terms of the potential energy change between trial (new) and existing (old) states and some other properties of the new and old configurations. Today, MC has developed to a powerful tool for simulating the properties of complex systems such as chain molecules, because of its capability to accelerate system equilibration through the implementation of large or unphysical moves that do not require the system to follow the natural trajectory.⁶⁷⁻⁷²

3.1. Reduction of computer generated polymer structures to networks of primitive paths

As discussed in B2, mapping simulation data onto the reptation model requires a reduction of computer generated polymer structures (either atomistic or in the coarse-grained representation of FENE-type descriptions) to networks of chain primitive paths by explicitly accounting for the entanglements or uncrossability constraints in the system.^{73,74} Such a task has been addressed in the last few years by a number of researchers. Kröger et al.⁷⁵ presented a single-chain projection operation methodology that makes use of two types of Hookean springs: the first type connects adjacent beads within the projected primitive path (PP) of the chain and the second the projected beads of the PP with the corresponding atoms of the original polymer chain. The coordinates of the PP are obtained by minimizing the total potential energy of the

springs, and the projection involves only a single parameter ζ , the ratio of the constants of the two springs which controls the contour length L of the PP.

The first method to extract the PP network simultaneously for *all* chains in a simulation box accounting also for entanglements, thus providing a microscopic foundation of the tube theory for high MW liquids, was presented by Everaers et al.⁷⁶ Everaers et al.⁷⁶ considered a bead-spring model of polymer chains with variable intrinsic stiffness and fixed chain ends in space. To reduce chain molecular conformations to conformations of primitive paths, only inter-chain excluded volume interactions were maintained so that chain crossing is prevented (the intra-chain ones were disabled in order to cause the chains to pull taut), and the energy of the system was minimized by gradually reducing the temperature to the zero Kelvin value, which eliminates thermal fluctuations. Such a methodology resulted in a mesh of primitive paths while automatically accounting for entanglements of arbitrary order, simultaneously for all chains in the system. Individual primitive paths consisted of straight segments of strongly fluctuating length and more or less sharp turns at entanglement points between different paths. Application of the method to a number of polymers led to accurate predictions of the plateau modulus and the packing length.⁷⁷⁻⁷⁹

More recently, Kröger⁸⁰ calculated primitive paths as “infinitely” thin and tensionless lines connecting the two ends of a polymer chain (considered as fixed in space), obtained under the constraint of chain un-crossability, by invoking geometric operations that minimize the contour length of the multiple disconnected path simultaneously for all chains present in the simulation cell (i.e., of the total contour length summed over all individual PPs). The algorithm (Z-code) and its newer version (Z1-code) return a solution which is robust against minor displacements of the disconnected path and chain relabeling. Foteinopoulou et al.⁸¹ used the algorithm to analyze entanglement statistics in model, atomistically detailed linear PE structures generated with the double-bridging Monte Carlo method (a chain connectivity algorithm capable of thermally equilibrating long polymethylene melts while maintaining monodispersity).⁸¹ Quantities computed include: (a) the distribution $p(Z)$ of the number of entanglements Z , (b) the distribution $p(N_e)$ of the entanglement spacing N_e , (c) the average inter-entanglement spacing $\langle N_e \rangle$ (average number of carbon atoms between successive entanglement points), (d) the distribution $p(L)$ of the contour length, and (e) the distribution $p(\alpha)$ of the step length α calculated through eq. (15) above, all as a function of chain length N . Typical results from more recent calculations with such an analysis with a number of *cis*-1,4 and *trans*-1,4-PB systems are shown in Figures 1-2.

A remarkable result of the topological analysis is that the distribution $p(Z)$ of the number of entanglements Z per chain can be accurately described by a simple expression of the form:

$$p(Z) = \frac{\langle Z-1 \rangle^{Z-1} e^{-\langle Z-1 \rangle}}{(Z-1)!} \quad (43)$$

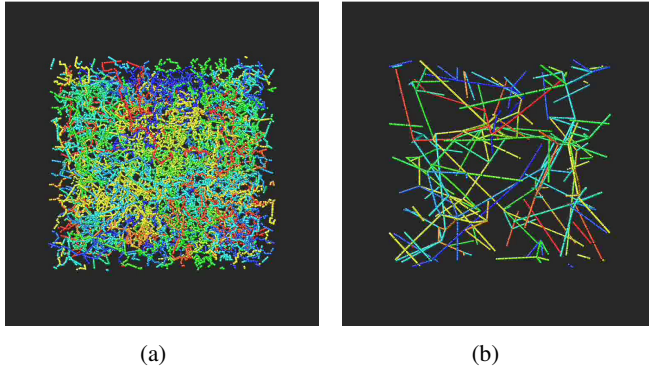


Figure 1: Reduction of an ensemble of atomistically represented chains (a) corresponding to a 32-chain C_{400} *trans*-1,4-PB melt at $T=413\text{K}$ and $P=1\text{atm}$ to an ensemble of primitive paths (b) with the shortest-path analysis (the Z1 algorithm) of Kröger.⁸⁰

i.e., by a Poisson distribution exactly as has been proposed by Schieber.⁸² Also, according to Schieber,⁸² Shanbhag-Larson,⁸³ and Zhou-Larson,⁸⁴ the scaled logarithm of the distribution $p(L)$ of the contour length L should be proportional to $U(L)$, the entropic potential governing PP length distribution:

$$p(L) \propto \exp\left[-\frac{U(L)}{k_B T}\right], \quad U(L) = \nu k_B T \left(\frac{L}{\langle L \rangle} - 1\right)^2 \quad (44)$$

where ν a constant with a strong chain length dependence, i.e., $\nu = \nu(N)$. By fitting eq. (44) to the results of the topological analysis for a number of simulated linear PE systems at $T=450\text{K}$, it has been found that ν is a decreasing function of chain length. For example, $\nu \approx 1.4$ for C_{320} PE, $\nu \approx 1.28$ for C_{500} PE, and $\nu \approx 1.1$ for C_{1000} PE, at $T=450\text{K}$.⁸¹

Tzoumanekas and Theodorou⁸⁵ have also presented a novel algorithm called CReTA (Contour Reduction Topological Analysis) for the reduction of an ensemble of computer generated atomistic polymer chains to a network of primitive paths. In CReTA, chains are represented as series of fused spheres, chain ends are held fixed, and primitive paths are defined as sequences of strings or strands containing chain atoms on straight segments. The algorithm involves random moves in which a string is randomly chosen and its atoms are displaced to corresponding equidistant points on the (same) segment joining the atoms on either side of the string. Chain crossing is avoided by rejecting moves leading to overlaps of the moved string atoms of a particular chain with any other atom belonging to a different chain. The moves lead to progressive shrinking of unentangled loops to straight strands composed of fused spheres which results in the reduction of the contour lengths simultaneously for all chains in the system. Application of CReTA to a number of model PE and *cis*-1,4-PB

melt systems produced results for the radial distribution function of entanglements and the distribution of the number of monomers between entanglements which, after proper rescaling, point to unified laws for certain descriptors of the underlying microscopic topological structure in the two systems.⁸⁵

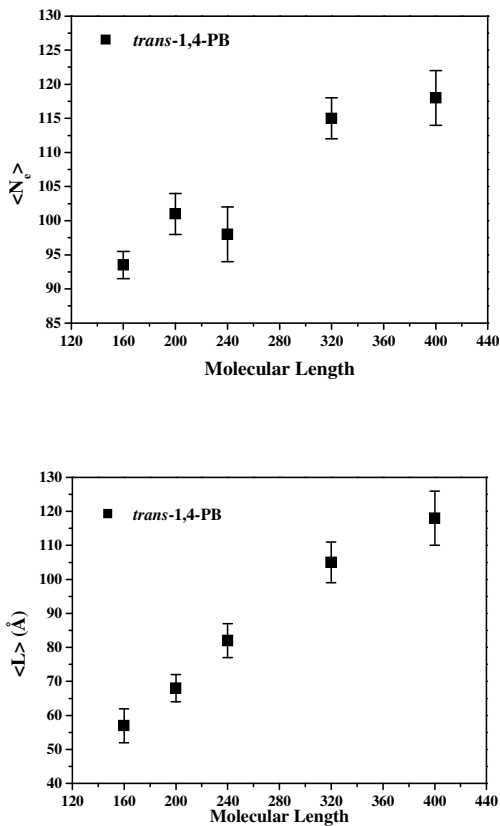


Figure 2: (a) Average entanglement spacing (in carbon atoms), and (b) average primitive path contour length, as a function of molecular length N (i.e., number of carbon atoms per chain) for *trans*-1,4-PB at $T=413\text{K}$ and $P=1\text{atm}$. The results have been obtained by applying the shortest-path analysis (the Z1 algorithm) of Kroger⁸⁰ on atomistically detailed model *trans*-1,4-PB systems.

3.2. The tube diameter

In the Doi-Edwards theory, the diameter d_t of the effective curvilinear tube (within which the motion of the chain is considered to be restricted) is of the same order as the step length α of the primitive chain. Thus, in the literature, the two quantities, α and d_t , are used practically interchangeably, allowing one to estimate d_t based on the statistical properties of the network of primitive paths generated through the computational reduction methods discussed above. Öttinger,⁸⁶ on the other hand, has analyzed the statistical properties of entangled polymer chains on the assumption of a Gaussian model for the polymer conformation and concluded that for infinitely-long, entangled polymer chains, strictly speaking, the value of d_t is almost one half that of α , i.e., $d_t = \frac{\alpha}{2}$. One way to calculate the precise value of d_t from computer simulations is to monitor the msd of atomistic segments perpendicularly to the chain original primitive path (the primitive path at time $t=0$) and compute d_t from the intersection of the two sub-curves marking the onset of tube constraints.⁸⁸ Such a method has been followed by Stephanou et al.⁸⁷ for three polymers (linear PE, *cis*-1,4-PB and *trans*-1,4-PB) yielding d_t values equal to 34.2 ± 0.43 Å for a C₅₀₀ PE melt at 450K, 33.0 ± 0.37 Å for a C₄₀₀ *trans*-1,4-PB melt at 413K, and 31.3 ± 1.07 Å for a C₄₀₀ *cis*-1,4-PB melt at 413K.⁸⁹

Alternatively, one can obtain an estimate of the (effective) tube diameter through the formula suggested by Likhtman and McLeish,⁸⁸ namely, $d_t = \sqrt{3\phi^*} = \sqrt{3\phi_n(t^*)}$, where $\phi_n(t)$ denotes the mean-square displacement of chain segments up to time t and obeys the four characteristic scalings discussed in Section 2.2 [see eq. (19)]. Here, t^* is the time where fitted straight lines through the first two scaling laws in the logarithmic plots of the segmental msd curves against time cross each other, and ϕ^* the corresponding msd value. As noted by Likhtman and

McLeish, $t^* = \frac{\pi^3}{36} \tau_e$. Figure 3 presents typical $\phi_n(t)$ -vs.- t curves in a log-log plot

obtained from equilibrium MD simulations with two *trans*-1,4-PB melts, an unentangled C₁₂₈ and an entangled C₃₂₀ system. The curve corresponding to the C₁₂₈ system (dashed line) is typical of a Rouse-like behavior: for times t shorter than the longest relaxation or Rouse time τ_1 , $\phi_n(t)$ scales with time as $\phi_n(t) \sim t^{0.50}$, i.e., in agreement with what is calculated by the Rouse model for diffusion in free space, whereas for times $t \gg \tau_1$, $\phi_n(t) \sim t$, since the distribution of $\mathbf{R}_n(t) - \mathbf{R}_n(0)$ becomes Gaussian with variance equal to $2Dt$ (D denoting the self-diffusion constant). In contrast to the C₁₂₈ melt, the $\phi_n(t)$ -vs.- t curve for the C₃₂₀ *trans*-1,4-PB system (solid line) shows the three distinct breaks (marked by the arrows in Figure 3) characteristic of reptation dynamics. It is also interesting to note that the values 0.50 ± 0.03 , 0.35 ± 0.03 , 0.55 ± 0.05 and 1.00 ± 0.08 , respectively, obtained from the MD simulations with the C₃₂₀ *trans*-1,4 PB melt for the slopes of the curves in the four regimes quantifying the power-law dependence of $\phi_n(t)$ on t compare remarkably well with the values 0.50, 0.25, 0.50 and 1 of the reptation theory [eq. (19)]. $\phi_n(t)$ -vs.- t plots similar to those of Figure 3 have also been reported in the literature by Harmandaris-Mavrantzas for linear PE⁹⁰ and by Karayiannis-Mavrantzas for H-shaped PE melts.⁹¹

By using then the Likhtman-McLeish formula $d_t = \sqrt{3\phi^*} = \sqrt{3\phi_n(t^*)}$, estimates of the tube diameter d_t were obtained (similar to those mentioned above), which compare quite well with experimentally reported data in the literature,⁹²⁻⁹⁸ according to which $d_t = 32.8 \text{ \AA}$ for linear PE (at 413K) and $d_t = 43.0 \text{ \AA}$ for *cis*-1,4-PB (at 298K).

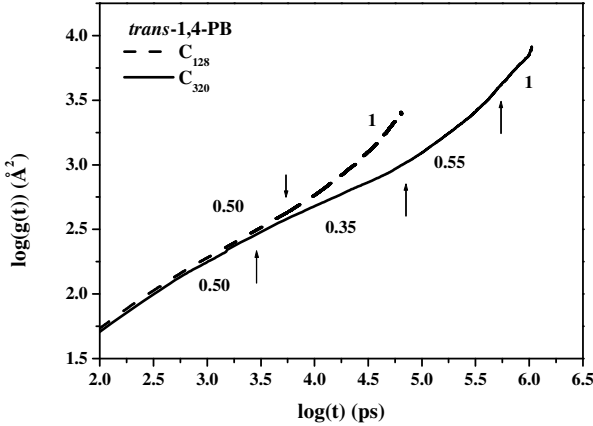


Figure 3: MD simulation results for the mean square displacement of the innermost chain segments against time in a log-log for a C₁₂₈ and a C₃₂₀ *trans*-1,4-PB system, at $T=413\text{K}$ and $P=1\text{atm}$. For the entangled C₃₂₀ system, one can distinguish the 3 characteristic breaks, as predicted by the Doi-Edwards reptation theory.

The tube diameter can also be calculated through neutron-spin-echo (NSE) measurements of the type reported by Wischniewski et al.⁹⁹⁻¹⁰¹ The analysis is based on the following analytical expression for the single-chain dynamic structure factor in the deep-reptation regime:¹⁰²⁻¹⁰⁴

$$\frac{S(q,t)}{S(q,0)} = \left\{ 1 - \exp\left[-(qd_t/6)^2\right] \right\} \exp(t/\tau_0) \operatorname{erfc}\left(\sqrt{t/\tau_0}\right) + \frac{8}{\pi^2} \exp\left[-(qd_t/6)^2\right] \sum_{p=\text{odd}} \frac{1}{p^2} \exp\left(-\frac{p^2 t}{\tau_d}\right) \quad (45)$$

where τ_0 is a short time constant given by $\tau_0 = 12\zeta/k_b T b^2 q^4$. Equation (45) has been derived on the basis of negligible CLF and CR phenomena, so it should be expected to be applicable only in high MW melts (chain length $N > 100 N_e$) for which these

phenomena are expected to be less important, and for wavevectors q such that:

$$\frac{1}{\sqrt{\langle R^2 \rangle_0}} \ll \frac{q}{2\pi} \ll \frac{1}{d_t}. \text{ For a } C_{1000} \text{ PE melt, for example, for which } \langle R^2 \rangle_0 \cong 19,500 \text{ \AA}^2,$$

the regime of q values for which one can use eq. (45) is $0.045 \ll q \ll 0.16$. $S(q,t)$ -vs.- t graphs for the C_{1000} melt corresponding to two such q values (equal to 0.08 \AA^{-1} and 0.10 \AA^{-1} , respectively) are shown in Figure 3 of Ref. 90. The symbols in that Figure describe the data directly obtained from the equilibrium MD simulations (symbols) while the lines indicate the predictions of the reptation theory based on the use of eq. (45). The letter were obtained by fitting the equation to the simulation data using as the only free parameter the value of the effective tube diameter α . The values of the other two parameters that appear in the equation, the friction factor ζ governing the short time scale τ_0 and the disentanglement time τ_d , were calculated according to the methodology described in Section 2.1 as $\zeta \cong 4 \times 10^{-10} \text{ dyn sec/cm}$, and $\tau_d \cong 4.5 \text{ \mu s}$, respectively. [ζ was extracted by mapping MD data for the chain self diffusion coefficient in the unentangled regime (e.g., for a C_{78} PE system) onto the Rouse model using also that its value should be chain-length independent since it refers to one monomer along a PE chain, while τ_d was estimated by extracting a value for the chain self-diffusion coefficient in the C_{1000} PE melt from the msd of the chain centre-of-mass in the Fickian regime based on the Einstein relation ($D \approx 0.00013 \text{ \AA}^2/\text{ps}$), and then using that $\tau_d = \frac{\langle R^2 \rangle_0}{3\pi^2 D}$]. With the above-mentioned values for ζ and τ_d , the simulation

curves in Figure 3 of Ref. 90 were fitted to eq. (45) leaving as the only free parameter the value of the effective tube diameter d_t . This led to the data shown by the continuous lines in Figure 3 of Ref. 90, with the best-fit value for d_t equal to $(55 \pm 5) \text{ \AA}$. As mentioned above, the corresponding experimental value for high MW linear PE melts is between 35 and 45 \AA .⁹⁹⁻¹⁰⁴ The comparison is favorable considering also that C_{1000} is a rather short PE melt (chain length approximately equal to $10 N_e$) whereas the predictions of the classical reptation theory should hold for extremely high MW systems (chain length $\sim 100 N_e$) due to the neglect of phenomena related to CLF and CR mechanisms.

3.3. Relation between the characteristic relaxation times τ_e , τ_R and τ_d

Atomistic MD simulation results can also be used to test analytic expressions reported in the literature relating the three characteristic times τ_e , τ_R and τ_d . For example, as noted by Ramos et al.,¹⁰⁵ a phenomenological relationship proposed by Graessley¹⁰⁶ on the basis of the Doi-Edwards theory suggests that:

$$\tau_d = \frac{15}{4} \frac{M}{M_e} \tau_R \quad (46)$$

which has been modified by Milner¹⁰⁷ and Milner-McLeish^{108,109} to

$$\tau_d = 3\tau_e \frac{M}{M_e} \left[1 - k \left(\frac{M_e}{M} \right)^{0.5} \right]^2 \quad (47)$$

to account for CLF with k a numerical constant of order unity. According to Doi^{110,111} and Ketzmerick and Öttinger,¹¹² $k=1.47$, while according to Likhtman and McLeish,⁸⁸ $k=1.69$.

3.4. The shear modulus of relaxation $G(t)$

From the Statistical Mechanics point of view, the shear stress modulus of relaxation can be calculated from the time autocorrelation function of the off-diagonal components of the instantaneous stress tensor by invoking the Green-Kubo relationship.¹¹³

$$G(t) = \frac{V}{k_B T} \langle \sigma_{ij}(t) \sigma_{ij}(0) \rangle, \quad i \neq j \quad (48)$$

In principle, the instantaneous stress tensor $\boldsymbol{\sigma}(t)$ that is needed in this equation can be obtained by an equilibrium MD simulation with the model system under study, using the virial theorem. Unfortunately, because of the strong fluctuations in the values of the off-diagonal components of $\boldsymbol{\sigma}(t)$, extremely long configurational averaging is required in order to calculate $G(t)$ with the required accuracy. In the literature, calculations of $G(t)$ for polymers based on the above expression for atomistic systems have been reported by Mondello and Grest.¹¹⁴ Harmandaris et al.¹¹⁵ have also used eq. (48) to directly calculate $G(t)$ for a C₂₄ and a C₇₈ PE system but that was possible only for times less than 10 ps; for longer times, the statistical noise in the calculated $\langle \sigma_{ij}(t) \sigma_{ij}(0) \rangle$ time autocorrelation function values was too large to allow for any meaningful results to be obtained. Harmandaris et al.¹¹⁵ also observed that the value of $G(t)$ at time $t=0$ was about 9.0×10^9 Pa, which is somewhat higher than the value of 1.0×10^9 Pa characterizing the relaxation modulus of polymers in the glassy regime.

One way to overcome the difficulties associated with the use of eq. (48) is to reconstruct $G(t)$ by resorting to the expressions provided by the Rouse and reptation theories, according to eqs. (5a) and (18b), respectively, presented in Section 2.1. This has been pursued quite extensively in the past yielding $G(t)$ curves which, although model-dependent, provide a satisfactory description of the true relaxation modulus of unentangled polymers. Harmandaris et al.,¹¹⁵ for example, found that for times beyond 10ps eq. (5a) provides results which seem to constitute a smooth continuation of the curve obtained with the direct application of the Green Kubo equation. In a very recent simulation study, such a method of reconstructing $G(t)$ for a number of entangled polymer melts guided by a mesoscopic molecular model of polymer dynamics parameterized on the basis of computer simulation studies was utilized by Ramos et al.¹⁰⁵ They exploited the results of atomistic equilibrium MC and MD simulations to obtain estimates of the entanglement molecular weight M_e and entanglement relaxation time τ_e (marking the onset of tube constraints on segmental dynamics) of a set of linear

C₁₀₀₀ PE models; these were next used as input to the following set of analytical expressions:

$$\begin{aligned}
 G(t) &= G_N^0 \left[\sum_i w_i \mu_i(t) \right]^2 \\
 G_N^0 &= \frac{4 \rho RT}{5 M_e} \\
 \mu_i(t) &= \frac{8}{\pi^2} \left[1 - k \left(\frac{M_e}{M_i} \right)^{0.5} \right] \sum_{p:odd} \frac{1}{p^2} \exp \left[-\frac{p^2 t}{\tau_{d,i}} \right] \\
 \tau_{d,i} &= 3\tau_e \left(\frac{M_i}{M_e} \right) \left[1 - k \left(\frac{M_e}{M_i} \right)^{0.5} \right]^2
 \end{aligned} \tag{49}$$

of the reptation theory modified to account for CLF and polydispersity effects (w_i is the weight fraction of species i with molecular weight M_i in the melt) to get $G(t)$.¹¹⁶⁻¹¹⁸ The computed $G(t)$ -vs.- t curves were found to compare favorably with experimentally measured ones on a CVO Bohlin torsion rheometer.

In a more recent study, Stephanou et al.⁸⁷ presented a methodology which leads directly to the calculation of all linear viscoelastic (LVE) properties of entangled polymer melts. The method involves the following steps: (a) First, an estimate is obtained for the average tube diameter d_t or tube radius α in the entangled melt based either on the maximum displacement of PP points perpendicularly to the tube axis at short times or on value of the segmental mean square displacement (msd) at the intersection of the curves in the log-log plot denoting the regimes of the early anomalous diffusion in free space and the Rouse dynamics.² Knowing the value of d_t or α , the original tube around each PP is constructed. (b) The time displacement of PP points perpendicularly to the axis of the original PP is monitored, and this is used to decide whether or not a segment s along the PP (s takes values between 0 and 1) has escaped the tube. Let x be the shortest distance of the segment from the axis of the original PP after time t : if $x > \alpha$, s has escaped the original tube (constructed at $t=0$) whereas if $x \leq \alpha$ it is still confined within the original tube. In fact, in the latter case, one has to be more careful since it should also be checked if the given point s has escaped from the tube laterally. This will have happened if the distance by which the segment s has diffused up to time t is larger than the remaining distance from s to either end of the PP at time $t=0$. This is more probable to occur for points s close to the two ends of the PP but as time goes by it applies to all segments s . By averaging over all PPs in the system and over a large number of accumulated trajectories, such an analysis allows the calculation of the probability $\psi(s,t)$ that a segment s has remained in the original tube after time t . (c) Having calculated the function $\psi(s,t)$, then the linear viscoelastic properties of the melt are obtained by making use of eqs. (18a)-(18e) of the reptation theory described in Section 2.2. For the calculation of the plateau modulus G_N^0 , and in order to emphasize CLF effects which are quite important for moderately entangled polymers, Stephanou et al.⁸⁷ have made use of the following equation,

$$G_N^0 = \frac{4}{5} \frac{\rho RT}{M} \frac{\langle L \rangle}{\alpha} \left[1 - \sqrt{\frac{\langle L^2 \rangle}{\langle L \rangle^2}} - 1 \right] \text{ where } M \text{ is the MW of the polymer, } \rho \text{ its density,}$$

and α the step length of the PP defined according to eq. (15) as $\alpha = \frac{\langle R^2 \rangle_0}{\langle L \rangle}$, while the term in the brackets on the right-hand-side accounts for corrections due to CLF. Typical results for the spectra $G'(\omega)$ and $G''(\omega)$ from these calculations for a number of *cis*-1,4-PB systems and for the zero-shear rate viscosity of a number of linear PE melts as a function of chain length were found to be in excellent agreement with experimental data from direct rheological measurements shifted to the same temperature.

A third way to obtain $G(t)$ is by monitoring the stress relaxation of pre-strained polymer configurations through a series of MD simulations in an extended statistical ensemble where, in addition to temperature and number of atoms, certain components of the stress tensor and/or the simulation cell are kept constant, exactly as described in Section 2.1. The method has its origin on the principles of polymer dynamics, where $G(t)$ is interpreted as the function that describes the way in which the shear stress relaxes after a sudden shearing displacement for a generalized linear viscolastic fluid:

$$G(t-t_0) = \frac{\sigma_{xy}(t)}{\gamma_0} \quad (50)$$

where γ_0 is the imposed sudden displacement and t_0 denotes the time instance at which the sudden deformation is applied. Although, strictly speaking, the method as described here has not been employed in MD simulations, variants have already appeared in the literature. Harmandaris et al.,¹¹⁵ for example, carried out a series of MD simulations of the relaxation of well-equilibrated PE configurations that had been pre-strained by means of the novel GENERIC MC algorithm under conditions that mimic a steady-state uniaxial elongational flow. By removing then the field, monitoring the relaxation of the melt back toward its field-free, quiescent state with MD in a suitable statistical ensemble, and mapping the results onto the solution of the Rouse model for the same physical experiment, Harmandaris et al.¹¹⁵ were able to deduce the relaxation modulus of a C₂₄ and a C₇₈ PE melt. Mapping onto the Rouse model was unavoidable in their case, since the initial state of the melt in the MD simulations corresponded not to the sudden shearing displacement discussed above but to a melt under conditions of steady-state uniaxial elongational flow. The MD stress relaxation experiments took place in the $nTL_x\sigma_y\sigma_{zz}$ ensemble where the following variables are kept constant: The number of atomistic units n , the temperature T , the length L_x of the simulation cell in the stretching direction (x), and the two normal (yy and zz) components of the stress tensor σ (equal to $-P_{\text{atm}}$). In practice, these are the macroscopic conditions encountered following the process of fiber spinning at the end of the spinning operations when the fibers are kept at constant extension and the stress

σ_{xx} in the direction of pulling is allowed to relax from its initial value to the equilibrium, field-free value of $-P_{\text{atm}}$.

3.5. The friction coefficient ζ – The diffusion coefficient D

For unentangled polymer melts, estimates of the segmental friction factor ζ can be obtained by mapping atomistic MD data either for the chain longest (chain end-to-end) relaxation time τ_R (obtained directly from the simulations by monitoring the decay of the time autocorrelation function for the chain end-to-end vector) or the chain center-of-mass self-diffusion coefficient D (obtained by monitoring the average msd of the chain center-of-mass) onto eqs. (3) and (4) of the Rouse model, respectively, as a function of chain length. The two estimates are denoted as ζ_r and ζ_D , respectively, and earlier MD simulation data with short PE melts^{119,120} showed them to be practically equal to each other, thus in the literature only a single value of ζ per carbon atom is usually reported. Figure 4 shows a typical plot of the chain length dependence of ζ for linear PE at $T=450\text{K}$ and *cis*-1,4-PB at $T=413\text{K}$, as obtained with such a mapping from MD simulations with a number of (different chain-length) systems. It is observed that ζ is a strong function of chain length for relatively short molecular lengths (less than about C_{90} for both PE and *cis*-1,4-PB), indicating that the Rouse model cannot accurately describe the dynamics of unentangled polymer melts in this range, with a constant, chain-length-independent friction coefficient value. This is due to chain end effects that contribute significantly to the system dynamics necessitating the consideration of additional relaxation mechanisms. Indeed, a modified Rouse theory accounting for the excess free volume near chain ends in such short chain length systems offers a more realistic description of the system dynamics.¹²¹ Figure 4 also shows that for chain lengths between C_{90} and C_{160} for both polymers, the Rouse theory (without any corrections for end effects) provides a better, more satisfactory description of the system dynamics.

For entangled polymer melts, an estimate of the segmental friction coefficient is possible only if simulation data for the longest relaxation time or the chain center of mass diffusivity are mapped onto the reptation model through a reduction of atomistically detailed chain configurations to a description based on the ensemble of PPs. Using then eqs. (18f) and (18e) of the reptation theory, one can extract reliable estimates of ζ also for chain lengths above the characteristic entanglement chain length. The results obtained are shown in Figure 4 by the open symbols and are seen to constitute a smooth continuation of the friction factor data obtained from the MD mapping onto the Rouse model. That reptation theory can describe the dynamics of the simulated PE and *cis*-1,4-PB systems above N_e with the same (chain-length-independent) value of the monomer friction factor as that extracted from the Rouse theory applied on shorter chain length systems ($N < N_e$) points to the validity and adequacy of the theory for long enough polymers; it further signals the crossover from the unentangled (or Rouse-like) to the entangled regime of polymer melt dynamics.

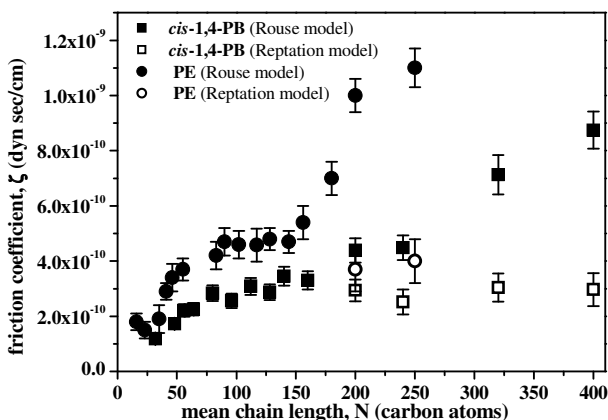


Figure 4: Typical plot of the chain length dependence of the monomer friction coefficient ζ for linear PE at $T=450\text{K}$ and *cis*-1,4-PB at $T=413\text{K}$ and $P=1\text{atm}$, as obtained by mapping MD simulation results with a number of different chain-length systems onto the Rouse (filled symbols) and reptation (open symbols) models of polymer dynamics.^{120,89}

The results reported in Figure 4 for PE refer to the friction factor per carbon chain of strictly *linear* melts. Branched polymers (polymers, in particular, with long-chain branching) exhibit rheological properties that differ substantially from those of linear melts, especially in extensional flows where long-chain branching leads to extreme strain hardening. In contrast, the shear rheology of such long-chain branched (LCB) liquids is very shear thinning, much like that of unbranched, linear polymers or of polymers with side branches too short to entangle with surrounding chains.¹²²⁻¹³⁵ According to the idealized pom-pom model of Bishko et al.¹²³ and McLeish and Larson,¹²⁴ in melts of entangled branched polymers that constitute generalizations of the H-structure (a “crossbar” from the two ends of which a number q of branches emerge; H-polymers correspond to the limiting case of $q=2$), all fast relaxation is confined to the arms, while at long times all of the effective friction to the reptation motion of their backbones is located at the branch points (rather than being distributed relatively uniformly along the chain). According to the pom-pom model, stress relaxation in an H- or q -polymer is thus considered to proceed through a 3-stage mechanism: (a) path-length fluctuation in the dangling arms, controlled by the rapid Rouse motion of the chain ends along the tube, at early times; (b) rapid path-length fluctuations that cross over to an exponentially slow “activated diffusion” regime for the deeper arm fluctuations, at longer times; and (c) renormalized reptation of the crossbars in a dilated tube defined by their mutual entanglements, after the star-like arms have completely retracted.

Molecular simulations¹³⁶⁻¹⁵⁰ can greatly contribute to understanding the special rheology of these H- or q-shaped polymers by probing their short and long time dynamics, especially the rapid relaxation due to arm breathing and the slow branch point diffusion governing the sluggish diffusive motion of the entire H-molecule, through direct atomistic MD simulations with model H-shaped structures, thoroughly pre-equilibrated with novel MC techniques. Karayiannis and Mavrantzas,⁹¹ for example, have been able to track the different relaxation mechanisms exhibited by rather long H-shaped PE melts (denoted as H_xy with *x* and *y* representing the average number of carbon atoms per backbone and arm, respectively) through long MD simulations with a multiple time step algorithm that allowed accessing simulation times on the order of a few microseconds in some cases. A number of H_xy melts were simulated: a 40-chain H₄₈24, a 32-chain H₇₈24, a 24-chain H₇₈48, a 24-chain H₁₂₈24, a 16-chain H₁₂₈48, and a 16-chain H₃₀₀50 PE melt. To compare against the dynamics of linear analogue PE melts (melts of the same arm, backbone or total molecular length), several linear PE systems, ranging in molecular length from C₂₄ up to C₅₀₀, were also subjected to long MD simulations. Results for the long time dynamics of the simulated H-shaped polymers (see Figures 3-4 of Ref. 91) showing the time evolution of the mean square displacements (msd's) corresponding to the diffusive motion of the centers of mass of the chains, $\langle [R_G(t) - R_G(0)]^2 \rangle$, and of the two branch points, $\langle [R_b(t) - R_b(0)]^2 \rangle$ demonstrated that, for a given H-polymer melt, the msd of its center of mass follows astonishingly closely that of the branch points: For example, for the shorter H-polymer studied (H₄₈24), Figure 4a of Ref. 91 shows that the two msd curves ($\langle [R_G(t) - R_G(0)]^2 \rangle$ and $\langle [R_b(t) - R_b(0)]^2 \rangle$) travel in time exactly one next to other right from the beginning. For the longer systems (H₁₂₈24, H₁₂₈48, and H₃₀₀50), the same Figure shows that this happens after the initial period of the usual sub-diffusive behavior has elapsed. This result validates the main assumption of the pom-pom theory that, at long times, the effective friction to curvilinear motion is practically all located at the branch points (rather than distributed along the molecule's main backbone and branches).

Results for the chain length dependence of the self-diffusion coefficient, *D*, of the simulated melts, have been reported in Figure 5 of Ref. 91, showing again the gradual, very smooth change with chain length at an intermediate value of *N* (between C₁₄₀ and C₁₇₀) marking the passage from a Rouse- to a reptation-like behavior: For chain lengths *N* below C₁₄₀, chain end effects combine with Rouse dynamics to result in *D* values that exhibit a power-law dependence on *N* of the form $D \propto N^{-b}$ with $b=1.70 (\pm 0.05)$. For chain lengths *N* above C₁₇₀, reptation dynamics dominates chain mobility, resulting in *D* values that exhibit a stronger dependence on *N*, described again by a power-law of the form $D \propto N^{-b}$ but now with $b=2.20 (\pm 0.10)$. The value of 2.20 predicted for the exponent *b* is in agreement with experimental data reported by Pearson et al.,¹⁵¹ Lodge,¹⁵² Tao et al.,¹⁵³ and Wang,¹⁵⁴ not only for PE but also for many other polymers. Further, according to McLeish and Larson,¹²⁴ the values of the branch point diffusion coefficient, *D_b*, can be used to extract an estimate for the branch point friction coefficient, ζ_b , through an Einstein argument, namely, $\zeta_b = \frac{k_B T}{D_b}$. For the H-

In a more recent study, Stephanou et al.⁸⁷ extended the work of Harmandaris et al.¹²⁰ in the sense that they avoided using the analytical expression, eq. (18f), of the original Doi-Edwards theory for the calculation of η_0 that neglects CLF and CR mechanisms; instead, they first computed the function $\psi(s,t)$ describing the remaining probability for a segment s along the primitive path in the original tube after time t , and then integrated it twice to calculate η_0 , according to the more fundamental expression, the first equality in eq. (18d). The results are shown in Figure 5 by the filled circles and seem to provide a very satisfactory description of the rheological measurements.^{151,120}

3.7. The viscosity function $\eta = \eta(\dot{\gamma})$

To calculate the full viscosity curve but also the rest of the material functions, one has to explicitly simulate the polymer melt under study in the presence of a flow field.¹⁵⁵ As discussed in Section 2.3, NEMD simulation studies of shear and planar elongational flow for polymers have been possible today with the help of a number of algorithms such as the DOLLS, SLOD, G-SLODD, and p-SLOD ones. With the p-SLOD algorithm, in particular, whose equations satisfy Newton's law, Baig et al.¹⁵⁶⁻¹⁵⁸ have recently carried out NEMD simulations of a number of short alkane melts such as decane (C₁₀H₂₂), hexadecane (C₁₆H₃₄), and tetracosane (C₂₄H₅₀) in shear (using the Lees-Edwards boundary conditions) and planar extension (using the Kraynik-Reinelt boundary conditions), and compared their results with the predictions of a number of well-known viscoelastic models for linear polymers; these included the UCM, the Rouse, the FENE-P, the extended White/Metzner (EWM), and the Giesekus models. The comparison was made both at the level of the (extra) stress tensor $\boldsymbol{\sigma}$ and at the level of the (dimensionless) conformation tensor $\tilde{\mathbf{c}}$. From a statistical mechanics point of view, the conformation tensor is obtained by averaging over individual chains, whereas the stress tensor is a collective property of the system (i.e., as a whole). Thus, $\tilde{\mathbf{c}}$ is considered as a more fundamental property than $\boldsymbol{\sigma}$, and it is the primary structural parameter used in the generalized bracket and GENERIC formalisms of non-equilibrium thermodynamics. The simple UCM model predicted reasonably well the linear viscoelastic properties (such as the first normal stress coefficient in the linear regime), but as expected failed to follow any of the nonlinear viscoelastic properties (such as the shear thinning of the viscosity and the non-zero second normal stress coefficient). The Rouse model, by incorporating multiple-modes of relaxation, was found to predict even better the linear viscoelastic properties of the simulated alkanes; however, being also a linear model, it could not predict any of the nonlinear viscoelastic properties. By accounting for the finite length of real chain molecules, the FENE-P model appeared to capture quite well the nonlinear viscoelasticity, its predictions being better for the case of planar extension than for the case of shear. In planar extension, Baig et al.¹⁵⁶⁻¹⁵⁸ also observed that, although the model can predict the tension-thinning behavior of the second elongational viscosity, it suggests a tension-thickening behavior (rather than a tension-thinning one as seen in the simulation results) for the first elongational viscosity. Furthermore, the model failed to predict the non-zero second normal stress coefficient in shear. The EWM model is similar to the UCM model but assumes a relaxation time that is a function of the conformation tensor in order to capture nonlinear viscoelasticity. Consequently, the

model could capture the shear-thinning behavior of the viscosity and of the first normal stress coefficient in shear, and the tension-thinning behavior of the two elongational viscosities in planar extension. Like the FENE-P, however, it incorrectly predicted a zero second normal stress coefficient, inconsistently with the simulation results. Baig et al.¹⁵⁶⁻¹⁵⁸ observed that, by far, the best comparison between NEMD simulation data and model predictions were noted for the Giesekus model. The model, based on the assumption of an anisotropic hydrodynamic drag coefficient in the constitutive equation, was capable of capturing many of the non-linear viscoelastic properties of the simulated alkanes. It captured the concave shape of the \tilde{c}_{xx} component of the conformation tensor, it could quantitatively follow the monotonic increase of \tilde{c}_{xx} and the monotonic decrease of \tilde{c}_{yy} with shear rate, the shear-thinning of the viscosity and of the first normal stress coefficient, the non-zero value of the second normal stress coefficient and its shear-thinning, and the ratio of the second to the first normal stress coefficient in shear. The model predictions were also encouraging in the case of planar extension, since it captured the tension-thinning of the two viscosities. The only major drawback of the Giesekus model was its inability to follow the nonlinear change of the \tilde{c}_{zz} component of the conformation tensor in the two flows and the saturation in the value of the \tilde{c}_{xx} component at high enough shear rates.

Baig et al.¹⁵⁶⁻¹⁵⁸ investigated also the relationship between stress and conformation tensors in the two flows in the light of the linear relationship considered in most viscoelastic models incorporating only intramolecular entropic effects (in connection with the assumption of a Gaussian model for chain molecules). Overall, the $\tilde{\mathbf{c}}$ -vs.- $\boldsymbol{\sigma}$ relationship was seen to be nonlinear, especially at high shear rates. For the shear flow, the curves appeared to follow the non-linear equation incorporated in the FENE-P model (which explains, to some extent, the success of this model in shear), but this was not the case for the planar extensional flow. Clearly, a simple linear relationship between $\boldsymbol{\sigma}$ and $\tilde{\mathbf{c}}$ is not applicable for arbitrary flows.

3.8. Birefringence

That the stress tensor does not depend linearly on the conformation tensor was demonstrated in a more recent study by Stephanou et al.⁵³ who proposed a generalized constitutive equation for the family of viscoelastic models that employ the conformation tensor as the pertinent structural variable. The new model incorporates terms that account for anisotropic hydrodynamic drag in the form suggested by Giesekus, finite chain extensibility with non-linear molecular stretching, non-affine deformation, and variation of the longest chain relaxation time with chain conformation. The new model was seen to fit quite satisfactorily the shear and planar extension NEMD simulation data of Baig et al.¹⁵⁶⁻¹⁵⁸ for the dependence of the conformation tensor on the applied shear or extensional rate. However, when the comparison was made at the level of the stress tensor, systematic deviations were observed between the two sets of data pointing out to the inadequacy of a simple linear law to capture the true $\tilde{\mathbf{c}}$ -vs.- $\boldsymbol{\sigma}$ relationship. To shed more light on this, Ionescu et al.^{29,30} have carried out a series of GENERIC MC simulations and the results were

used to numerically calculate the elastic energy through thermodynamic integration. The results were found to be consistent with the form of the Booij expression:⁴⁷

$$\Delta A(\tilde{\mathbf{c}}) \propto \frac{1}{2} \int \left[\text{tr}(\tilde{\mathbf{c}} - \mathbf{I}) - \ln(\det \tilde{\mathbf{c}}) \right] dV \quad (51)$$

for the free energy of deformation, provided that for each shear rate the latter is calculated using the simulation data for the conformation tensor and not the model predictions (see Section 3.10 below). This confirms that it is not the expression for the free energy in eq. (35c) that is faulty but the constitutive or evolution law (or the assumptions made to derive the specific form of the constitutive model).

Also in an effort to understand the conditions under which a linear relationship should be expected between stress and conformation tensors, Mavrantzas and Theodorou¹⁵⁹ have presented a direct calculation of the birefringence of uniaxially stretched PE melts, providing a measure of the induced anisotropy at the monomer level. By transforming the polarizability tensor of each individual skeletal bond (or united atom group) from the coordinate frame of its principal axes to the laboratory frame, the ensemble average polarizability tensor per methylene group $\langle \mathbf{a} \rangle$ of uniaxially stretched polymer melts was calculated as a function of the segment order parameter S_x . And from that, the anisotropic melt refractive index $\Delta n (= n_{xx} - n_{yy})$ was obtained by employing a tensorial form of the Clausius–Mossotti and Lorentz–Lorentz relationships.¹⁵⁹ Numerical results for two linear PE melts (average chain length C_{78} and C_{200}) by Mavrantzas and Theodorou¹⁵⁹ confirmed the validity of the stress optical law for small enough imposed elongational flow rates. The calculated stress optical law coefficient C was found to be equal to $(3.15 \pm 0.20) \times 10^{-9} \text{ Pa}^{-1}$ for the C_{78} and equal to $(2.35 \pm 0.10) \times 10^{-9} \text{ Pa}^{-1}$ for the C_{200} PE melt. These results compare quite favorably with the experimental observations according to which, for high MW and high density, linear PE melts, C comes out to be independent of the MW and of the applied elongational flow rate, equal to $C_{\text{exp}} = 2.20 \times 10^{-9} \text{ Pa}^{-1}$. Mavrantzas and Theodorou also computed the birefringence of a shorter C_{24} PE melt over a wide range of field strengths generating stress values that extend from a few decades up to a few hundreds of atmospheres (i.e., this system was simulated both in the linear and non-linear regime).¹⁵⁹ The stress optical law was observed to be violated when the tensile stress exceeded roughly 20 MPa. The reason for this breakdown was the distortion of chains towards strongly elongated intrinsic shapes in response to favorable lateral intermolecular interactions. This issue is discussed in more detail in Section 3.10 below. Additional simulation results for the birefringence of deformed PE melts have been presented in the more recent study by Baig et al.¹⁵⁸

3.9. The relaxation matrix

In Section 2.3, we reviewed how atomistic simulation data obtained with the GENERIC MC simulation method can be mapped onto the generalized constitutive equation representative of the family of conformation tensor viscoelastic models. Figure 6 gives an idea of the quality of the information that can be obtained from such a mapping.

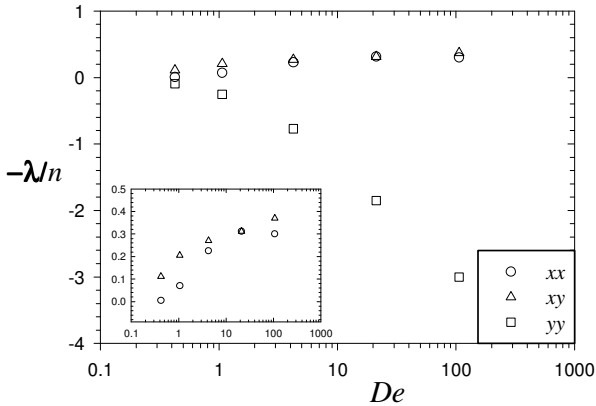


Figure 6: The values of the xx , xy and yy components of the tensorial thermodynamic field α or λ ($\alpha = -\lambda/n$, where n is the number of chains per volume) as a function of the imposed (dimensionless) shear rate that brings GENERIC MC and direct NEMD simulation results for the (dimensionless) conformation tensor \tilde{c} of a C_{50} linear PE melt on top of each other ($T=450K$).^{28,160}

What is shown in the Figure is how, given a shear rate, one should choose the non-zero components of the tensor α (or, equivalently, λ) in a GENERIC MC simulation in order to generate the true shear flow in a short (unentangled) $C_{50}H_{102}$ PE melt. All simulations²⁸ have been executed in the semi-grand canonical ensemble⁶⁷ with the end-bridging Monte Carlo algorithm⁶⁸ using 120 chains of $C_{50}H_{102}$ in a periodic rectangular box with dimensions ($xx \times yy \times zz$) of $93 \times 45 \times 45 \text{ \AA}^3$ (x denotes the flow direction, y the velocity gradient direction, and z the neutral direction) with the SKS⁶² united-atom force-field. Results are reported for 5 different non-equilibrium states corresponding to 5 different values of the Deborah (De) number, equal to 0.425, 1.06, 4.25, 21.3, and 106. De has been defined as the product of the imposed shear rate $\dot{\gamma}_0$ and the longest relaxation (Rouse) time of the system, λ_0 ; for the $C_{50}H_{102}$ PE melt, $\lambda_0 \approx 0.5 \text{ ns}$ as estimated by the integral below the curve describing the time decay of the autocorrelation function for the chain end-to-end vector.²⁸ In all simulations, the temperature T was equal to 450 K and the mass density ρ equal to 0.744 g/cm^3 . The values of the xx , xy and yy components of the tensor α (or λ) shown in the Figure and their variation with De are clearly different from those expected according to the UCM model [see eq. (38) above] or to the Giesekus model [see eq. (39) above] for reasonable values of the Giesekus parameter β . Using the values of the tensor λ (or α) reported in Figure 6, the resulting predictions for the non-zero components of the

conformation tensor $\tilde{\mathbf{c}}$ obtained from the GENERIC MC simulations are shown in Figure 7.

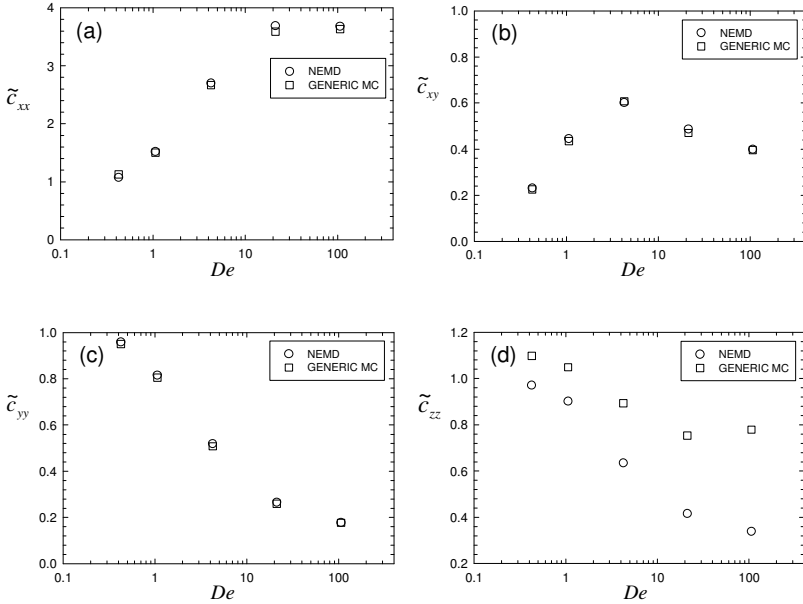


Figure 7: Comparison of the values of the components \tilde{c}_{xx} , \tilde{c}_{xy} , \tilde{c}_{yy} , and \tilde{c}_{zz} of the conformation tensor $\tilde{\mathbf{c}}$ as obtained from the GENERIC MC simulations with the values of the tensorial field \mathbf{a} (or, equivalently, $\boldsymbol{\lambda}$) reported in Figure 6 and from a direct application of the NEMD method, as a function of the imposed De number ($T=450K$).^{28, 160}

In the Figure, we also show the results for $\tilde{\mathbf{c}}$ obtained through a direct application of the NEMD method for each dimensionless shear rate. As seen, \tilde{c}_{xx} , \tilde{c}_{xy} , and \tilde{c}_{yy} from the GENERIC MC simulations practically coincide with the corresponding values from the NEMD simulations for all five shear rates studied. The same was found to be true for the birefringence. These results confirm that the new, thermodynamically-guided GENERIC MC methodology is capable of generating the true non-equilibrium structure in the system for the given shear flow. It is only for the

\tilde{c}_{zz} component of the conformation tensor $\tilde{\mathbf{c}}$ (displayed in Figure 7d) that a disagreement is observed between MC and NEMD results. This is related to the choice of a zero value for the zz component of the tensor $\boldsymbol{\lambda}$ (or, equivalently, $\boldsymbol{\alpha}$) as suggested by expression (42) for the relaxation matrix underlying most of the currently available conformation tensor viscoelastic models, which apparently seems to be not an appropriate choice. To reproduce exactly also \tilde{c}_{zz} , the more general expression, eq. (41), for the tensors $\boldsymbol{\alpha}$ or $\boldsymbol{\lambda}$ involving a non-zero zz component should have been incorporated in the GENERIC MC simulations.¹⁶⁰ The main conclusion from these simulations is therefore that the rather general form of the friction matrix, eq. (36), for this family of models needs to be improved under either the generalized bracket or the GENERIC formalisms of non-equilibrium thermodynamics, by allowing for a non-zero value of α_{zz} (or λ_{zz}). This is quite important, since α_{zz} (or λ_{zz}) is directly related with the capability of the model(s) to predict a non-zero second normal stress coefficient in simple shear.

3.10. The free energy of a deformed polymer melt

By its very definition, the tensor $\boldsymbol{\alpha}$ is directly related to the (non-equilibrium) free energy of the system – see eq. (35b) above. Indeed, eq. (35b) allows one to accurately calculate the free energy of a simulated deformed polymer melt through thermodynamic integration by requiring a series of simulations over the thermodynamic state points, by varying one component of $\boldsymbol{\alpha}$ and fixing the rest. Knowing the free energy of the system at non-equilibrium states is extremely useful in the theoretical development of non-equilibrium thermodynamics, as well as in developing viscoelastic models with enhanced predictive capability. Although work is still in progress in this direction, a few useful results have already been reported. Mavrantzas-Theodorou,²⁶ for example, have calculated the free energy ΔA of deformed short PE melts (of chain length C_{24} and C_{78} , respectively) subjected to a homogeneous extensional flow at constant elongation rate in one direction only (which has perhaps the simplest kinematical structure in nonequilibrium MC simulations of flowing systems). By partitioning ΔA into an energetic and an entropic component, Mavrantzas-Theodorou²⁶ also showed that the melt response to the applied elongational field is purely entropic only for long chains and low orienting fields, causing chains merely to orient along the direction of the flow while leaving their intrinsic shape practically unaltered. In contrast, for melts of short chain lengths and for high orienting fields, where the chain intrinsic shape becomes more elongated and attractive lateral interchain interactions are intensified, a significant energetic contribution develops.

More recently, Ionescu et al.²⁹⁻³⁰ carried out a detailed analysis of the response of linear PE systems ranging in molecular length from C_{24} to C_{78} to an applied field under conditions that a uniaxial extensional flow is generated by accessing strain rates significantly larger than those achieved by Mavrantzas-Theodorou, and over a range of temperatures (from 300K to 450K). They demonstrated clear contributions of energetic effects to the elasticity of the system, which in turn manifested in a conformationally dependent heat capacity (which is significant under large deformations). Violations of the hypothesis of purely entropic elasticity⁴⁶⁻⁵² were

evident in these simulations, wherein the free energy of the system was demonstrated to be composed of significant energetic effects under high degrees of orientation arising mainly from favorable intermolecular side-to-side interactions developing in the process of elongation due to chain uncoiling and alignment in the direction of extension. Figure 5 of Ref. 30, for example, presents results from these simulations referring to the variation of chain specific Helmholtz free energy for the unentangled C₃₆ linear PE system as function of field strength α_{xx} and temperature T .

Ionescu et al.²⁹⁻³⁰ investigated also the individual contributions of bonded and non-bonded interactions to the total internal energy of the deformed PE systems. The bonded interactions are represented by the angle bending and torsion interaction potentials, while the non-bonded interactions are represented by the 12-6 LJ pair interaction potential which can further be split into intramolecular and intermolecular contributions. Figure 6 of Ref. 30 shows the individual component contributions to the total internal energy change for a C₂₄ system at $T=400\text{K}$, as a function of α_{xx} . It is seen that: (i) the two components of the non-bonded energy (intra- and intermolecular) are of opposite sign and different in magnitude, (ii) the orienting field has almost no effect on the angle-bending energy, (iii) the torsional energy decreases because the lower energy *trans* dihedral conformations of the extended chains are enhanced, and (iv) changes in torsional and intramolecular potential energies are of about the same magnitude and opposite sign, thus essentially offsetting each other. Overall, and unless extreme conditions are applied causing chains to get fully extended configurations, it is evident from Figure 6 of Ref. 30 that the most important contributor to the change in total energy is the intermolecular LJ energy. In contrast, therefore, to the total internal energy of a single isolated chain which may not change with extension (due to the two components discussed above offsetting each other), the internal energy of an ensemble of chains will change significantly due to favorable side-to-side interchain interactions, which lower the overall internal energy. Macroscopically, this will translate into additional energy being generated within the material, increasing the temperature of the fluid. Such an aspect has been confirmed by the experimental observations described by Ionescu et al.,²⁹ in which the calculated temperature increase due to deformation under the purely entropic elasticity assumption is under-predicted by up to 100% at the highest values of strain rate.

Ionescu et al.³⁰ also calculated the Helmholtz free energy change ΔA from the simulation data via thermodynamic integration and compared their results against the predictions of the Booiij expression, eq. (51) above, assumed in the UCM, PTT and Giesekus viscoelastic models. For all values of the molecular weight and temperature investigated, excellent agreement between the simulation data and the Booiij free energy expression was demonstrated (see Figure 7a of Ref. 30). These molecular simulation findings for the elasticity of unentangled polymer melts and the dependence of ΔA on α_{xx} suggest that any inadequacy of deferential viscoelastic models to fit rheological data (obtained, e.g., from GENERIC MC or NEMD simulations) will most probably be due not to the form of the free energy function invoked by the model but due either to the form of the relaxation matrix incorporated in the model (e.g., we saw that expression (36) above fails to generate a non-zero value for the zz element of the tensor α) or to the rather simple formula, eq. (35c), used to relate stress and conformation tensors in these models.

3.11. Molecular mechanism of liquid slip

NEMD simulations have also been employed in order to investigate if slip occurs and how during the flow of a liquid near a bounding solid.¹⁶¹⁻¹⁷¹ For example, quite recently, Martini et al.¹⁷¹ have reported results from NEMD simulations of a short alkane melt in a planar Couette flow supporting two mechanisms of slip. The simulated model liquid consisted of 96 n-decane molecules modeled in a united atom description (i.e., each molecule was assumed to be composed of ten monomers connected by rigid bonds) allowing also for bond bending and torsion, in a channel width of 3 nm. It was sheared by moving the top and bottom bounding walls at velocities $+U$ and $-U$, respectively, with magnitude U between 1 and 1000 m s⁻¹. The potential field generated by the solid (modeled as a Lennard-Jones interaction) gives rise to an adsorption layer which the liquid atoms preferentially occupy. At low levels of forcing, Martini et al.¹⁷¹ observed that individual atoms in this first layer hop from one equilibrium site to another giving rise to what the authors call defect slip. [The first layer is defined as being composed of those liquid atoms whose centers of mass lie between the wall and the first minimum in the average liquid density profile. Density and velocity profiles were calculated by averaging the number and velocity of atoms in discrete bins parallel to the channel walls]. The defect slip was therefore associated with the localized hopping of only a few molecules that move along the liquid-solid interface in a non-linear mode, and is independent of the dynamics outside the local neighborhood of the wall. At high levels of forcing, Martini et al.¹⁷⁰ found that the entire layer slips, i.e., all atoms adjacent to the wall contribute to slip; this is called global slip. The NEMD simulations showed that the percentage of atoms engaged in slip remains small as long as the wall speed is less than about 10 m s⁻¹, but approaches 100% at a wall speed of several hundreds of m s⁻¹. The corresponding variation of the slip length L_s with wall speed was also shown in Ref. 171. [The slip length is quantified by the ratio $L_s = \frac{v_s}{\dot{\gamma}_0}$ where $\dot{\gamma}_0$ is the mean shear rate determined

by fitting a straight line through the average velocity profile in the central part of the channel, and v_s is the slip speed determined from the difference between the wall speed and $\dot{\gamma}_0$ extrapolated to the wall]. It was seen that the slip length increased with wall speed for speeds up to 10 m s⁻¹ beyond which it remained practically constant. The NEMD simulation predictions were supported from a theoretical model for slip based on a set of Frenkel-Kontorova (FK) equations.^{162,164} By allowing for changes in the population of the first layer due to atoms that move/diffuse into and out of it, a modified version of the equations was derived called the variable density Frenkel-Kontorova (vdFK) model.^{162,164,171} The model predicted a first bifurcation (critical point) at low forcing from no-slip to solitonic propagation of defects over a corrugated potential, as well as a second critical value at higher values of forcing corresponding to a global motion of the entire layer, exactly as was observed in the simulations.

4. CONCLUSIONS AND OUTLOOK

Despite the multiplicity of length and time scales characterizing structure and motion in polymers, atomistic simulations (by directly providing the link to microstructure) have turned nowadays to an indispensable tool for studying the

viscoelastic and rheological properties of polymeric systems and understanding the molecular mechanisms behind their distinct and unique mechanical response to an applied flow field compared to those of the simpler, Newtonian liquids. Through the development of a wealth of novel algorithms and methodologies (multiple-time step MD, GENERICMC, NEMD, etc.), in particular, they are capable of providing today: (a) direct estimates of the material functions in shear and elongation and how they depend on chain length and molecular architecture, (b) reliable estimates of the parameters entering theoretical models of polymer dynamics and rheology, (c) the true form of the free energy and relaxation matrices in thermodynamic descriptions of these systems beyond equilibrium as a function of a set of pertinent state variables, and (d) molecular-level validation of the key assumptions underlying popular and widely accepted theories.

In the near future, these efforts will be directed toward the development of models for targeted, industrially-relevant applications. By reducing the microstructural description offered by atomistic simulations to more coarse-grained levels involving: (a) mappings of atomistic trajectories onto primitive paths and then onto slip-link models, (b) parameterization of macroscopic constitutive equations on the information provided by the finer levels, and (c) systematic incorporation of the effect of mechanisms elucidated at finer levels into continuum models, the hope exists to be able to resolve long-standing issues in polymer simulation community with direct relevance to polymer producing and processing industries. Typical examples include: (a) the modeling of interfaces in nanostructured, high performance materials based on polymers and copolymers (e.g., for understanding deformation processes over multiple time and length scales when polymeric adhesives are debonded from an adherent), (b) the understanding of the mechanical properties of polymer nanocomposites and of heterogeneous (hybrid organic/inorganic) materials (e.g., materials containing nanoparticles and nanofillers), (c) the modeling of transport phenomena in nanostructured polymeric materials for the design of tailor-made membranes (for use in the area of waste gas or fluid separation, with significant environmental implications), and (d) the self-assembly properties of bio-inspired polymers for drug delivery and medical and gene encapsulation and release applications.

ACKNOWLEDGEMENTS

The author is grateful to Dr. Chunggi Baig, Dr. Georgia Tsolou, Dr. Vagelis Harmandaris, Dr. Nikos Karayiannis, Dr. Katerina Foteinopoulou, and Mr. Pavlos Stephanou for their research work in the last few years in Patras on many of the issues discussed in this Review Article. The author would also like to acknowledge the invaluable help of Dr. Georgia Tsolou, Mr. Pavlos Stephanou and Dr. Chunggi Baig in the preparation of the Figures of this Article.

REFERENCES

1. Rouse, P.E., *A theory of the linear viscoelastic properties of dilute solutions of coiling polymers*, J. Chem. Phys., 21 (1953) 1272-1280.
2. Doi, M., Edwards, S.F., *The theory of polymer dynamics* (Clarendon Press, Oxford, England, 1986).
3. Higgins, J., Benoit, H.C., *Polymers and neutron scattering* (Oxford University Press Inc., New York, 1996).
4. Yang, L., Srolovitz, D.J., Yee, A.F., *Extended ensemble molecular dynamics method for constant strain rate uniaxial deformation of polymer systems*, J. Chem. Phys., 107 (1997) 4396-4407.
5. de Gennes, P.G., *Reptation of a polymer chain in the presence of fixed obstacles*, J. Chem. Phys., 55 (1971) 572-579.
6. Doi, M., Edwards, S.F., *Dynamics of concentrated polymer systems I. Brownian motion in the equilibrium state*, J. Chem. Soc. Faraday Trans. 2, 74 (1978) 1789-1801.
7. Doi, M., Edwards, S.F., *Dynamics of concentrated polymer systems II. Molecular motion under flow*, J. Chem. Soc. Faraday Trans. 2, 74 (1978) 1802-1817.
8. Doi, M., Edwards, S.F., *Dynamics of concentrated polymer systems III. The constitutive equation*, J. Chem. Soc. Faraday Trans. 2, 74 (1978) 1818-1832.
9. McLeish, T.C.B., *Tube theory of entangled polymer dynamics*, Adv. Phys., 51 (2002) 1379-1527.
10. des Cloizeaux, J., *Double reptation vs. simple reptation in polymer melts*, Europhys. Lett., 5 (1988) 437-442.
11. Marrucci, G., *Relaxation by reptation and tube enlargement: A model for polydisperse polymers*, J. Polym. Sci.: Polym. Phys. Ed., 23 (1985) 159-177.
12. Marrucci, G., *Dynamics of entanglements: A nonlinear model consistent with the Cox-Merz rule*, J. Non-Newtonian Fluid Mech., 62 (1996) 279-289.
13. Watanabe, H., *Viscoelasticity and dynamics of entangled polymers*, Prog. Polym. Sci., 24 (1999) 1253-1403.
14. Phan-Thien N., Tanner, R.I., *A new constitutive equation derived from network theory*, J. Non-Newtonian Fluid Mech., 2 (1977) 353-365.
15. Phan-Thien, N., *A nonlinear network viscoelastic model*, J. Rheol., 22 (1978) 259-283.
16. Giesekus H., *A simple constitutive equation for polymer fluids based on the concept of deformation-dependent tensorial mobility*, J. Non-Newtonian Fluid Mech., 11 (1982) 69-109.
17. Larson R.G., *Constitutive equations for polymer melts and solutions* (Butterworth-Heinemann, London, 1988).

18. Wiest, J.M., *A differential constitutive equation for polymer melts*, Rheol. Acta, 28 (1989) 4-12.
19. Doufas, A.K., Dairanieh I.S., McHugh A.J., *A continuum model for flow-induced crystallization of polymer melts*, J. Rheol., 43 (1999) 85-109.
20. Doufas A.K., *Analysis of the rheotens experiment with viscoelastic constitutive equations for probing extensional rheology of polymer melts*, J. Rheol., 50 (2006) 749-769.
21. Peterlin A., *Hydrodynamics of macromolecules in a velocity field with longitudinal gradient*, J. Polym. Sci.: Polym. Lett., 4 (1966) 287-291.
22. Cohen A., *A Padé approximant to the inverse Langevin function*, Rheol. Acta, 30 (1991) 270-273.
23. Bird, R.B., Armstrong, R.C., Hassager, O., *Dynamics of polymeric liquids, Vol. 1, Fluid Mechanics*, 2nd ed. (Wiley-Interscience, New York, 1987).
24. Bird, R.B., Curtiss, C.F., Armstrong, R.C., Hassager, O., *Dynamics of polymeric liquids, Vol. 2, Kinetic Theory*, 2nd ed. (Wiley-Interscience, New York, 1987).
25. Housiadas K.D., Beris, A.N., *Extensional behavior influence on viscoelastic turbulent channel flow*, J. Non-Newtonian Fluid Mech., 140 (2006) 41-56.
26. Mavrantzas, V.G., Theodorou, D.N., *Atomistic simulation of polymer melt elasticity: Calculation of the free energy of an oriented polymer melt*, Macromolecules, 31 (1998) 6310-6332.
27. Mavrantzas, V.G., Öttinger, H.C., *Atomistic Monte Carlo simulations of polymer melt elasticity: Their nonequilibrium thermodynamics GENERIC formulation in a generalized canonical ensemble*, Macromolecules, 35 (2002) 960-975.
28. Baig, C., Mavrantzas, V.G., *Thermodynamically guided nonequilibrium Monte Carlo for generating realistic shear flows in polymeric systems*, Phys. Rev. Lett., 99 (2007) 257801.
29. Ionescu, T., Edwards, B.J., Keffer, D.J., Mavrantzas, V.G., *Energetic and entropic elasticity of nonisothermal flowing polymers: experiment, theory, and simulation*, J. Rheol., 52 (2008) 105-140.
30. Ionescu, T., Mavrantzas, V.G., Edwards, B.J., Keffer, D.J., *Atomistic simulation of energetic and entropic elasticity in short-chain polyethylenes*, J. Rheol., 52 (2008) 567-589.
31. Evans, D.J., Morriss, G.P., *Statistical Mechanics of non-equilibrium liquids* (Academic, New York, 1990).
32. Hoover, W.G., Evans, D.J., Hickman, R.B., Ladd, A.J.C., Ashurst, W.T., Moran, B., *Lennard-Jones triple-point bulk and shear viscosities. Green-Kubo theory, Hamiltonian mechanics, and nonequilibrium molecular dynamics*, Phys. Rev. A, 22 (1980) 1690-1697.
33. Evans, D.J., Morriss, G. P., *Nonlinear-response theory for steady planar Couette flow*, Phys. Rev. A, 30 (1984) 1528-1530.

34. Daivis, P.J., Todd, B.J., *A simple, direct derivation and proof of the validity of the SLLOD equations of motion for generalized homogeneous flows*, J. Chem. Phys., 124 (2006) 194103.
35. Tuckerman, M.E., Mundy, C.J., Balasubramanian, S., Klein, M.L., *Modified nonequilibrium molecular dynamics for fluid flows with energy conservation*, J. Chem. Phys., 106 (1997) 5615-5621.
36. Todd, B.D., Daivis, P.J., *The stability of nonequilibrium molecular dynamics simulations of elongational flows*, J. Chem. Phys., 112 (2000) 40-46.
37. Lees, W., Edwards, S.F., *The computer study of transport processes under extreme conditions*, J. Phys. C, 5 (1972) 1921-1929.
38. Kraynik, A.M., Reinelt, D.A., *Extensional motions of spatially periodic lattices*, Int. J. Multiphase Flow, 18 (1992) 1045-1059.
39. Todd, B.D., Daivis, P.J., *Nonequilibrium molecular dynamics simulations of planar elongational flow with spatially and temporally periodic boundary conditions*, Phys. Rev. Lett., 81 (1998) 1118-1121.
40. Todd, B.D., Daivis, P.J., *Nonlinear shear and elongational rheology of model polymer melts by non-equilibrium molecular dynamics*, J. Non-Newtonian Fluid Mech., 111 (2003) 1-18.
41. Baig, C., Edwards, B.J., Keffer, D.J., Cohran, H.D., *A proper approach for nonequilibrium molecular dynamics simulations of planar elongational flow*, J. Chem. Phys., 122 (2005) 114103.
42. Edwards, B.J., Baig, C., Keffer, D.J., *An examination of the validity of nonequilibrium molecular-dynamics simulation algorithms for arbitrary steady-state flows*, J. Chem. Phys., 123 (2005) 114106.
43. Edwards, B.J., Baig, C., Keffer, D.J., *A validation of the p-SLLOD equations of motion for homogeneous steady-state flows*, J. Chem. Phys., 124 (2006) 194104.
44. Beris, A.N., Edwards, B.J., *Thermodynamics of flowing systems* (Oxford University Press, New York, 1994).
45. Öttinger, H.C., *Beyond equilibrium thermodynamics* (John Wiley & Sons, New Jersey, 2005)
46. Weiner, J.H., *Statistical mechanics of elasticity* (John Wiley & Sons, New York, 1983).
47. Booij, H.C., *The energy storage in the Rouse model in an arbitrary flow field*, J. Chem. Phys., 80 (1984) 4571-4572.
48. Astarita, G., *Thermodynamics of dissipative materials with entropic elasticity*, Polym. Eng. Sci., 14 (1974) 730-733.
49. Flory, P.J., *Principles of polymer chemistry* (Cornell University Press, Ithaca, New York, 1953).
50. Treloar, L.R.G., *The Physics of rubber elasticity* (3rd ed., Clarendon: Oxford, U.K., 1975).

51. Astarita, G., Sarti, G.C., *The dissipative mechanism in flowing polymers: theory and experiments*, J. Non-Newtonian Fluid Mech., 1 (1976) 39-50.
52. Astarita, G., Sarti, G.C., *An approach to thermodynamics of polymer flow based on internal state variables*, Polym. Eng. Sci., 16 (1976) 490-495.
53. Stephanou, P.S., Baig, C., Mavrantzas, V.G., *A generalized differential constitutive equation for polymer melts based on principles of non-equilibrium thermodynamics*, J. Rheol., 2009 (in press).
54. Allen, M.P., Tildesley, D.J., *Computer simulation of liquids* (Oxford University Press, Oxford, 1987).
55. Sadus, R.J., *Molecular simulation of fluids: Theory, algorithms and object-orientation* (Elsevier, Amsterdam, 1999).
56. Tuckerman, M.E., Berne, B.J., Martyna, G.J., *Reversible multiple time scale molecular dynamics*, J. Chem. Phys., 97 (1992) 1990-2001.
57. Plimpton, S.J., *Fast parallel algorithms for short-range molecular dynamics*, J. Comp. Phys., 117 (1995) 1-19.
58. Martyna G.J., Tuckerman M.E., Tobias, D.J., Kein, M.L., *Explicit reversible integrators for extended systems dynamics*, Mol. Phys., 87 (1996) 1117-1157.
59. Harmandaris, V.A., Mavrantzas, V.G. "Molecular dynamics simulations of polymers". In: D.N. Theodorou and M.J. Kotelyanskii (eds.) *Simulation methods for modeling polymers*, Marcel Dekker, 2002.
60. Karayiannis, N.Ch., Mavrantzas, V.G., Mouratidis, D., Chiotelis, E., Kyriassides, C.D. *Atomistic molecular dynamics simulation of short-chain branched polyethylene melts*. In: M. Laso and E. Perpete (eds.) *Polymer modeling at multiple time and length scales*, Elsevier, 2006.
61. van der Ploeg, P., Berendsen, J.C., *Molecular dynamics simulation of a bilayer membrane*, J. Chem. Phys., 76 (1982) 3271-3276.
62. Siepman, J.I., Karaborni, S., Smit, B., *Simulating the critical behavior of complex fluids*, Nature, 365 (1993) 330-332.
63. Toxvaerd, S., *Equation of state of alkanes II*, J. Chem. Phys., 107 (1997) 5197-5204.
64. Martin, M.G., Siepman, J.I., *Transferable potentials for phase equilibria. 1. United-atom description of n-alkanes*, J. Phys. Chem. B, 102 (1998) 2569-2577.
65. Nath, S.K., Escobedo, F.A., de Pablo, J.J., *On the simulation of vapor-liquid equilibria for alkanes*, J. Chem. Phys., 108 (1998) 9905-9911.
66. Metropolis, N., Rosenbluth, A.W., Rosenbluth, M.N., Teller, A.H., Teller, E., *Equation of state calculations by fast computing machines*, J. Chem. Phys., 21 (1953) 1087-1092.
67. Pant, P.V.K., Theodorou, D.N., *Variable connectivity method for the atomistic Monte Carlo simulation of polydisperse polymer melts*, Macromolecules, 28 (1995) 7224-7234.

68. Mavrantzas, V.G., Boone, T.D., Zervopoulou, E., Theodorou, D.N., *End-bridging Monte Carlo: A fast algorithm for atomistic simulation of condensed phases of long polymer chains*, Macromolecules, 32 (1999) 5072-5096.
69. Karayiannis, N.Ch., Mavrantzas, V.G., Theodorou, D.N., *A novel Monte Carlo scheme for the rapid equilibration of atomistic model polymer systems of precisely defined molecular architecture*, Phys. Rev. Lett., 88 (2002) 105503.
70. Theodorou, D.N., *Variable-connectivity Monte Carlo algorithms for the atomistic simulation of long-chain polymer systems*. In: P. Nielaba, M. Mareschal, and G. Ciccotti (eds.) *Bridging Time Scales: Molecular Simulations for the Next Decade*, Springer Verlag, Berlin, 2002.
71. Mavrantzas, V.G., *Monte Carlo simulation of chain molecules*. In: S. Yip (ed.) *The Encyclopaedia of the Advanced Materials*, Marcel Dekker, 2004.
72. Karayiannis, N.Ch., Mavrantzas, V.G., *Atomistic Monte Carlo methods for the atomistic simulation of polymers with a linear or a non-linear molecular architecture*. In: M. Laso and E. Perpete (eds.) *Polymer modeling at multiple time and length scales*, Elsevier, 2006.
73. Pütz, M., Kremer, K., Grest, G.S., *What is the entanglement length in a polymer melt?*, Europhys. Lett., 49 (2000) 735-741.
74. Padding, J.T., Briels, W.J., *Uncrossability constraints in mesoscopic polymer melt simulations: Non-Rouse behavior of $C_{120}H_{242}$* , J. Chem. Phys., 115 (2001) 2846-2859.
75. Kröger, M., Ramírez, J., Öttinger, H.C., *Projection from an atomistic chain contour to its primitive path*, Polymer, 43 (2002) 477-487.
76. Everaers, R., Sukumaran, S.K., Grest, G.S., Svaneborg, C., Sivasubramanian, A., Kremer, K., *Rheology and microscopic topology of entangled polymeric liquids*, Science, 303 (2004) 823-826.
77. Sukumaran, S., Grest, G.S., Kremer, K., Everaers, R., *Identifying the primitive path mesh in entangled polymer liquids*, J. Polym. Sci.: Part B: Polym. Phys., 43 (2005) 917-933.
78. Kremer, K., Sukumaran, S.K., Everaers, R., Grest, G.S., *Entangled polymer systems*, Comp. Phys. Commun., 169 (2005) 75-81.
79. Uchida, N., Grest, G.S., Everaers, R., *Viscoelasticity and primitive path analysis of entangled polymer liquids: From F-actin to polyethylene*, J. Chem. Phys., 128 (2008) 044902.
80. Kröger, M., *Shortest multiple disconnected path for the analysis of entanglements in two- and three-dimensional polymeric systems*, Comp. Phys. Comm., 168 (2005) 209-232.
81. Foteinopoulou, K., Karayiannis, N.Ch., Mavrantzas, V.G., Kröger, M., *Primitive path identification and entanglement statistics in polymer melts: Results from direct topological analysis on atomistically detailed polyethylene models*, Macromolecules, 39 (2006) 4207-4216.

82. Schieber, J., *Fluctuations in entanglements of polymer liquids*, J. Chem. Phys., 118 (2003) 5162-5166.
83. Shanbhag, S., Larson, R.G., *Chain retraction in a fixed entanglement network*, Phys. Rev. Lett., 94 (2005) 076001.
84. Zhou, Q., Larson, R.G., *Direct calculation of the tube potential confining entangled polymers*, Macromolecules, 39 (2006) 6737-6743.
85. Tzoumanekas, C., Theodorou, D.N., *Topological analysis of linear polymer melts: A statistical approach*, Macromolecules, 39 (2006) 4592-4604.
86. Öttinger, H.C., *Coarse-graining of wormlike polymer chains for substantiating reptation*, J. Non-Newtonian Fluid Mech., 120 (2004) 207-213.
87. Stephanou, P.S., Baig, C., Tsolou, G., Mavrantzas, V.G., Kröger, M., *Quantifying chain reptation in entangled polymer melts: Topological and dynamical mapping of atomistic simulation results onto the tube model*, Macromolecules, submitted (2009).
88. Likhtman, A.E., McLeish, T.C.B., *Quantitative theory for linear dynamics of linear entangled polymers*, Macromolecules, 35 (2002) 6332-6343.
89. Tsolou, G., Mavrantzas, V.G., Theodorou, D.N., *Detailed atomistic molecular dynamics simulation of cis-1,4-poly(butadiene)*, Macromolecules, 38 (2005) 1478-1492.
90. Harmandaris, V.A., Mavrantzas, V.G., *Segmental dynamics in polyethylene melts through atomistic molecular dynamics simulations*. In: A.F. Terzis and E. Paspalakis (eds.) *Recent research topics and developments in chemical physics: From quantum scale to macroscale*, ISBN: 978-81-7895-316-8, Transworld Research Network, Kerala, India, 2008.
91. Karayiannis, N.Ch., Mavrantzas, V.G., *Hierarchical modeling of the dynamics of polymers with a non-linear molecular architecture: Calculation of branch point friction and chain reptation time of H-shaped polyethylene melts from long molecular dynamics simulations*, Macromolecules, 38 (2005) 8583-8596.
92. Colby, R.H., Fetters, L.J., Graessley, W.W., *The melt viscosity-molecular weight relationship for linear polymers*, Macromolecules, 20 (1987) 2226-2237.
93. Fetters, L.J., Lohse, D.J., Richter, D., Witten, T.A., Zirkel, A. *Connection between polymer molecular weight, density, chain dimensions, and melt viscoelastic properties*, Macromolecules, 27 (1994) 4639-4647.
94. Ferry, J.D., *Viscoelastic properties of polymers* (John Wiley & Sons, New York, 1980).
95. Bueche, F., *Physical properties of polymers* (Interscience, New York, 1962).
96. Mark, J.E., *Polymer data handbook* (Oxford Univ. Press, New York, 1999).
97. van Krevelen, D.W., *Properties of polymers: Their estimation and correlation with chemical structure* (Elsevier Science Publication Co., Amsterdam, 1990).

98. Brandup, J., Immergut, E.H., *Polymer handbook* (John Wiley & Sons, New York, 1989).
99. Wischniewski, A., Richter, D., *Comment on "What is the entanglement length in a polymer melt?"*, Europhys. Lett., 52 (2000) 719-720.
100. Wischniewski, A., Monkenbusch, M., Willner, L., Richter, D., Likhtman, A.E., McLeish, T.C.B., Farago, B., *Molecular observation of contour-length fluctuations limiting topological confinement in polymer melts*, Phys. Rev. Lett., 88 (2002) 058301.
101. Wischniewski, A., Monkenbusch, M., Willner, L., Richter, D., Kali, G., *Direct observation of the transition from free to constrained single-segment motion in entangled polymer melts*, Phys. Rev. Lett., 90 (2003) 058302.
102. de Gennes, P.G., *Coherent scattering by one reptating chain*, J. Physique, 42 (1981) 735-740.
103. Smith, G.D., Paul, W., Monkenbusch, M., Willner, L., Richter, D., Qiu, X.H., Ediger, M. D., *Molecular dynamics of a 1,4-polybutadiene melt. Comparison of experiment and simulation*, Macromolecules, 32 (1999) 8857-8865.
104. Zamponi, M., Wischniewski, A., Monkenbusch, M., Willner, L., Richter, D., Likhtman, A.E., Kali, G., Farago, B., *Molecular observation of constraint release in polymer melts*, Phys. Rev. Lett., 96 (2006) 238302.
105. Ramos, J., Vega, J.F., Theodorou, D.N., Martinez-Salazar, J., *Entanglement relaxation time in polyethylene: Simulation versus experimental data*, Macromolecules, 41 (2008) 2959-2962.
106. Graessley, W.W., *Some phenomenological consequences of the Doi-Edwards theory of viscoelasticity*, J. Polym. Sci.: Polym. Phys. Ed., 18 (1980) 27-34.
107. Milner, S.T., *Relating the shear-thinning curve to the molecular weight distribution in linear polymer melts*, J. Rheol., 40 (1996) 303-315.
108. Milner, S.T., McLeish, T.C.B., *Parameter-free theory for stress relaxation in star polymer melts*, Macromolecules, 30 (1997) 2159-2166.
109. Milner, S.T., McLeish, T.C.B., *Reptation and contour-length fluctuations in melts of linear polymers*, Phys. Rev. Lett., 81 (1998) 725-728.
110. Doi, M., *Explanation for the 3.4 power law of viscosity of polymeric liquids on the basis of the tube model*, J. Polym. Sci.: Polym. Lett. Ed., 19 (1981) 265-273.
111. Doi, M., *Explanation for the 3.4-power law for viscosity of polymeric liquids on the basis of the tube model*, J. Polym. Sci.: Polym. Phys. Ed., 21 (1983) 667-684.
112. Ketzmerick, R., Öttinger, H.C., *Simulation of a non-Markovian process modelling contour length fluctuation in the Doi-Edwards model*, Continuum Mech. & Thermodyn., 1 (1989) 113-124.
113. McQuarrie, D.A., *Statistical mechanics* (HarperCollins Publishers, New York, 1976).

114. Mondello, M., Grest, G.S., *Viscosity calculations of n-alkanes by equilibrium molecular dynamics*, J. Chem. Phys., 106 (1997) 9327-9336.
115. Harmandaris, V.A., Mavrantzas, V.G., Theodorou, D.N., *Atomistic molecular dynamics simulation of stress relaxation upon cessation of steady-state uniaxial elongation flow*, Macromolecules, 33 (2000) 8062-8076.
116. Rubinstein, M., Helfand, E., Pearson, D.S., *Theory of polydispersity effects of polymer rheology: binary distribution of molecular weights*, Macromolecules, 20 (1987) 822-829.
117. Viovy, J.L., Rubinstein, M., Colby, R.H., *Constraint release in polymer melts: tube reorganization versus tube dilation*, Macromolecules, 24 (1991) 3587-3596.
118. Rubinstein, M., Colby, R.H., *Polymer Physics* (Oxford University Press, 2003).
119. Harmandaris, V.A., Mavrantzas, V.G., Theodorou, D.N., *Atomistic molecular dynamics simulation of polydisperse linear polyethylene melts*, Macromolecules, 31 (1998) 7934-7943.
120. Harmandaris, V.A., Mavrantzas, V.G., Theodorou, D.N., Kröger, M., Ramírez, J., Öttinger, H.C., Vlassopoulos, D., *Crossover from the Rouse to the entangled polymer melt regime: Signals from long, detailed atomistic molecular dynamics simulations supported by rheological experiments*, Macromolecules, 36 (2003) 1376-1387.
121. Harmandaris, V.A., Doxastakis, M., Mavrantzas, V.G., Theodorou, D.N., *Detailed molecular dynamics simulation of the self-diffusion of n-alkane and cis-1,4 polyisoprene oligomer melts*, J. Chem. Phys., 116 (2001) 436-446.
122. Doi, M., Kuzuu, N.Y., *Rheology of star polymers in concentrated solutions and melts*, J. Polym. Sci.: Polym. Lett. Ed., 18 (1980) 775-780.
123. Bishko, G., McLeish, T.C.B., Harlen, O.G., Larson, R.G., *Theoretical molecular rheology of branched polymers in simple and complex flows: The pom-pom model*, Phys. Rev. Lett., 79 (1997) 2352-2355.
124. McLeish, T.C.B., Larson, R.G., *Molecular constitutive equations for a class of branched polymers: The pom-pom polymer*, J. Rheol., 42 (1998) 81-110.
125. McLeish, T.C.B., Allgaier, J., Bick, D.K., Bishko, G., Biswas, P., Blackwell, R., Blottiere, B., Clarke, N., Gibbs, B., Groves, D.J., Hakiki, A., Heenan, R.K., Johnson, J.M., Kant, R., Read, D.J., Young, R.N., *Dynamics of entangled H-polymers: Theory, rheology, and neutron-scattering*, Macromolecules, 32 (1999) 6734-6758.
126. Lohse, D.J., Milner, S.T., Fetters, L.J., Xenidou, M., Hadjichristidis, N., Mendelson, R.A., Garcia-Franco, C.A., Lyon, M.K., *Well-defined, model long chain branched polyethylene. 2. Melt rheological behavior*, Macromolecules, 35 (2002) 3066-3075.
127. Bourrigaud, S., Marin, G., Poitou, A., *Shear modification of long-chain branched polymers: A theoretical approach using the pom-pom model*, Macromolecules, 36 (2003) 1388-1394.

128. Gabriel, C., Münstedt, H., *Strain hardening of various polyolefins in uniaxial elongational flow*, J. Rheol., 47 (2003) 619-630.
129. McLeish, T.C.B., *Molecular rheology of H-polymers*, Macromolecules, 21 (1988) 1062-1070.
130. Roovers, J., *Melt rheology of H-shaped polystyrenes*, Macromolecules, 17 (1984) 1196-1200.
131. Shie, S.C., Wu, C.T., Hua, C.C., *Nonlinear stress relaxation of H-shaped polymer melt revisited using a stochastic pom-pom model*, Macromolecules, 36 (2003) 2141-2148.
132. Lee, J.H., Fetters, L.J., Archer, L.A., *Stress relaxation of branched polymers*, Macromolecules, 38 (2005) 10763-10771.
133. Archer, L.A., Juliani, *Linear and nonlinear viscoelasticity of entangled multiarm (pom-pom) polymer liquids*, Macromolecules, 37 (2004) 1076-1088.
134. Doeringhaus, P.J., Baird, D.G., *Assessing the branching architecture of sparsely branched metallocene-catalyzed polyethylenes using the pom-pom constitutive model*, Macromolecules, 35 (2002) 10087-10095.
135. Kapnistos, M., Vlassopoulos, D., Roovers, J., Leal, L.G., *Linear rheology of architecturally complex macromolecules: Comb polymers with linear backbones*, Macromolecules, 38 (2005) 7852-7862.
136. Daivis, P.J., Evans, D.J., Morriss, G.P., *Computer-simulation study of the comparative rheology of branched and linear alkanes*, J. Chem. Phys., 97 (1992) 616-627.
137. Mondello, M., Grest, G.S., *Molecular dynamics of linear and branched alkanes*, J. Chem. Phys., 103 (1995) 7156-7165.
138. Mondello, M., Grest, G.S., Garcia, A.R., Silbernagel, B.G., *Molecular dynamics of linear and branched alkanes: Simulations and nuclear magnetic resonance results*, J. Chem. Phys., 105 (1996) 5208-5215.
139. Khare, R., de Pablo, J., Yethiraj, A., *Rheological, thermodynamic, and structural studies of linear and branched alkanes under shear*, J. Chem. Phys., 107 (1997) 6956-6964.
140. Kostov, K.S., Freed, K.F., Webb III, E.B., Mondello, M., Grest, G.S., *Dynamics of linear and branched alkane melts: Molecular dynamics test of theory for long time dynamics*, J. Chem. Phys., 108 (1998) 9155-9167.
141. Martin, M.G., Siepmann, J.I., *Novel configurational-bias Monte Carlo method for branched molecules. Transferable potentials for phase equilibria. 2. United-atom description of branched Alkanes*, J. Phys. Chem. B, 103 (1999) 4508-4517.
142. MacDowell, L.G., Vega, C., Sanz, E., *Equation of state of model branched alkanes: Theoretical predictions and configurational bias Monte Carlo simulations*, J. Chem. Phys., 115 (2001) 6220-6235.

143. Nath, S.K., Khare, R., *New forcefield parameters for branched hydrocarbons*, J. Chem. Phys., 115 (2001) 10837-10844.
144. Zacharopoulos, N., Economou, I.G., *Morphology and organization of poly(propylene imine) dendrimers in the melt from molecular dynamics simulation*, Macromolecules, 35 (2002) 1814-1821.
145. Jabbarzadeh, A., Atkinson, J.D., Tanner, R.I., *Effect of molecular shape on rheological properties in molecular dynamics simulation of star, H, comb, and linear polymer melts*, Macromolecules, 36 (2003) 5020-5031.
146. Bosko, J.T., Todd, B.D., Sadus, R.J., *Internal structure of dendrimers in the melt under shear: A molecular dynamics study*, J. Chem. Phys., 121 (2004) 1091-1096.
147. Bosko, J.T., Todd, B.D., Sadus, R.J., *Viscoelastic properties of dendrimers in the melt from nonequilibrium molecular dynamics*, J. Chem. Phys., 121 (2004) 12050-12059.
148. Peristeras, L.D., Economou, I.G., Theodorou, D.N., *Structure and volumetric properties of linear and triarm star polyethylenes from atomistic Monte Carlo simulation using new internal rearrangement moves*, Macromolecules, 38 (2005) 386-397.
149. Peristeras, L.D., Rissanou, A.N., Economou, I.G., Theodorou, D.N., *Novel Monte Carlo molecular simulation scheme using identity-altering elementary moves for the calculation of structure and thermodynamic properties of polyolefin blends*, Macromolecules, 40 (2007) 2904-2914.
150. Ramos, J., Peristeras, L.D., Theodorou, D.N., *Monte Carlo simulation of short chain branched polyolefins in the molten state*, Macromolecules, 40 (2007) 9640-9650.
151. Pearson, D.S., Ver Strate, G., Von Meerwall, E., Schilling, F.C., *Viscosity and self-diffusion coefficient of linear polyethylene*, Macromolecules, 20 (1987) 1133-1141.
152. Lodge, T.P., *Reconciliation of the molecular weight dependence of diffusion and viscosity in entangled polymers*, Phys. Rev. Lett., 83 (1999) 3218-3221.
153. Tao, H., Lodge, T.P., von Meerwall, E.D., *Diffusivity and viscosity of concentrated hydrogenated polybutadiene solutions*, Macromolecules, 33 (2000) 1747-1758.
154. Wang, S.Q., *Chain dynamics in entangled polymers: Diffusion versus rheology and their comparison*, J. Polym. Sci., Polym. Phys., 41 (2003) 1589-1604.
155. Morriss, G.P., Daivis, P.J., Evans, D.J., *The rheology of normal alkanes: decane and eicosane*, J. Chem. Phys., 94 (1991) 7420-7433.
156. Baig, C., Edwards, B.J., Keffer, D.J., Cohran, H.D., *Rheological and structural studies of liquid decane, hexadecane, and tetracosane under planar elongational flow using nonequilibrium molecular-dynamics simulations*, J. Chem. Phys., 122 (2005) 184906.

157. Baig, C., Edwards, B.J., Keffer, D.J., Cochran, H.D., Harmandaris, V.A., *Rheological and structural studies of linear polyethylene melts under planar elongational flow using nonequilibrium molecular dynamics simulations*, J. Chem. Phys., 124 (2006) 084902.
158. Baig, C., Jiang, B., Edwards, B.J., Keffer, D.J., Cochran, H.D., *A comparison of simple rheological models and simulation data of n-hexadecane under shear and elongational flow*, J. Rheol., 50 (2006) 625-640.
159. Mavrantzas, V.G., Theodorou, D.N., *Atomistic Monte Carlo simulation of steady-state uniaxial, elongational flow of long-chain polyethylene melts: dependence of the melt degree of orientation on stress, molecular length and elongational strain rate*, Macromol. Theory Simul., 9 (2000) 500-515.
160. Baig, C., Mavrantzas, V.G., *T Multiscale simulation of polymer melt viscoelasticity guided from nonequilibrium statistical thermodynamics: Atomistic Non-Equilibrium Molecular Dynamics coupled with Monte Carlo in an expanded statistical ensemble*, Phys. Rev. B, submitted (2008).
161. Blake, T.D., *Slip between a liquid and a solid: D.M. Tolstoi's (1952) theory reconsidered*, Colloids Surfaces, 47 (1990) 135-145.
162. Floría, L.M., Mazo, J.J., *Dissipative dynamics of the Frenkel-Kontorova model*, Adv. Phys., 45 (1996) 505-598.
163. Thompson, P.A., Troian, S.M., *A general boundary condition for liquid flow at solid surfaces*, Nature, 389 (1997) 360362.
164. Braun, O.M., Kivshar, Y.S., *Nonlinear dynamics of the Frenkel-Kontorova model*, Phys. Rep., 306 (1998) 1-108.
165. Sokhan, V.P., Nicholson, D., Quirke, N., *Fluid flow in nanopores: An examination of hydrodynamic boundary conditions*, J. Chem. Phys., 115 (2001) 3878-3887.
166. Lichter, S., Roxin, A., Mandre, S., *Mechanisms for liquid slip at solid surfaces*, Phys. Rev. Lett., 93 (2004) 086001.
167. Urbakh, M., Klafter, J., Gourdon, D., Israelachvili, J., *The nonlinear nature of friction*, Nature, 389 (2004) 360-362.
168. Martini, A., Liu, Y.C., Snurr, R.Q., Wang, Q., *Molecular dynamics characterization of thin film viscosity for EHL simulation*, Trib. Lett., 21 (2006) 217-225.
169. Lichter, S., Martini, A., Snurr, R.Q., Wang, Q., *Liquid slip as a rate process*, Phys. Rev. Lett., 98 (2007) 226001
170. Bocquet, L., Barrat, J.-L., *Flow boundary conditions from nano- to microscales*, Soft Matter, 3 (2007) 685693.
171. Martini, A., Roxin, A., Snurr, R.Q., Wang, Q., Lichter, S., *Molecular mechanisms of liquid slip*, J. Fluid Mech., 600 (2008) 257-269.